Western Kentucky University
TopSCHOLAR®

5-1-2012

Hybrid Nanostructures for Artificial Machine Olfaction

Landon Joseph Oakes

Western Kentucky University, landon.oakes879@topper.wku.edu

Follow this and additional works at: http://digitalcommons.wku.edu/theses

Part of the Physics Commons

HYBRID NANOSTRUCTURES FOR ARTIFICIAL MACHINE OLFACTION

A Thesis
Presented to
The Faculty of the Department of Physics
Western Kentucky University
Bowling Green, Kentucky

In Partial Fulfillment
Of the Requirement for the Degree
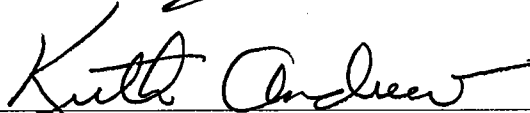Master of Science

By
Landon Joseph Oakes

May 2012

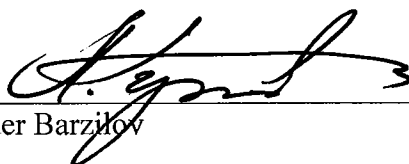HYBRID NANOSTRUCTURES FOR ARTIFICIAL MACHINE OLFACTION

Date Recommended 5-8-12

Vladimir Dobrokhotov, Director of Thesis

Keith Andrew

Alexander Barzilov

Kinchel C Doerner 18-May-2012

Director, Graduate Studies and Research   Date

TABLE OF CONTENTS

LIST OF FIGURES

HYBRID NANOSTRUCTURES FOR ARTIFICIAL MACHINE OLFACTION

Landon Oakes   May 2012   55 pages

Directed by: Dr. Vladimir Dobrokhotov, Dr. Alexander Barzilov and Dr. Keith Andrew

Department of Physics and Astronomy   Western Kentucky University

The detection of low level concentrations of particles in a gaseous environment is of importance to many fields, especially Homeland Security. The ability to identify ppb concentrations of explosives and their degradation products can aid in the detection of improvised explosive devices (IEDs), ammunition dumps, or hidden explosives. One method of accomplishing this task is through the use of an array of chemiresistors in an electronic nose device. For this study, chemiresistors were constructed using 3-D silica nanospring mats with a contiguous film of ZnO nanocrystals and ZnO nanocrystals decorated by metallic nanoparticles. Samples with an average grain size of 15nm were found to be the most responsive and upon exposure to a gas flow of 20% O_2 and 80% N_2 with ~200 ppm of acetone and an operational temperature of 400 ^{o}C produced a relative change in conductance by a factor of 400. The addition of metal nanoparticles onto the surface of the ZnO nanocrystals produced a relative change in conductance by a factor of 1100. Under optimum conditions, sensing elements of this design exhibited well-defined spikes in conductance upon exposure to explosive vapors (TNT, TATP) at the ppb levels. The use of a pattern recognition system allowed discrimination between three analyte chemicals.

Chapter 1: Introduction

The ability to identify small concentrations of chemical compounds in the atmosphere is of utmost importance to the Department of Homeland Security and the United States Armed Forces. Small concentrations of specific compounds may be indicative of dangerous materials such as explosives or chemical warfare agents. The detection of low-level concentrations of vapor has application in nearly all areas of Homeland Security, including: personnel security, facility security, border security, and incident response.

To date, identifying small concentrations of chemical compounds in the field has proved troublesome and expensive with existing technologies [1]. Currently, biological olfactory techniques (i.e. canines) are employed as the least expensive method for performing this task. In a biological olfactory system, an atmospheric sample is pre-concentrated, or "sniffed" and odorants within the sample bind to receptors in the nose. These receptors then send a signal to the olfactory bulb for processing and a processed signal is sent to the brain for identification. The brain uses past experiences with similar odorants to perform classification [42,43].

Using a technique such as the canine olfactory system to perform trace vapor detection is inherently costly due to the time required for training, limited range of detectable chemicals for each canine, and the inability to quantify results [43]. For these reasons, an electronic analogue to the canine, referred to as an electronic nose, has been the subject of much research. In an electronic nose system, odorants are pre-concentrated and electrochemically react with an array of sensors to generate a conductometric signal. This signal is sent to a pre-processing algorithm in which discriminatory features may be

1

extracted and used in a pattern recognition system for odorant classification. Such a pattern recognition system classifies an odorant by comparing the features of the generated signal with a library of similar features accumulated from previous exposures to known odorants [34-36]. This process for creating an electronic nose signature and its similarity with the biological olfactory system can be seen in figure 1.1.

The focus of this study is to demonstrate the feasibility of using solid-state materials as sensor elements in an electronic nose system. In this paper, the feasibility of using nanospring sensing elements in an electronic nose system is presented as a function of both sensitivity and selectivity. Sensitivity is defined as the lowest detectable concentration of a chemical species and selectivity is defined by a number of popular pattern recognition techniques. The results from this work have been published in multiple peer reviewed journals [2,3,44].
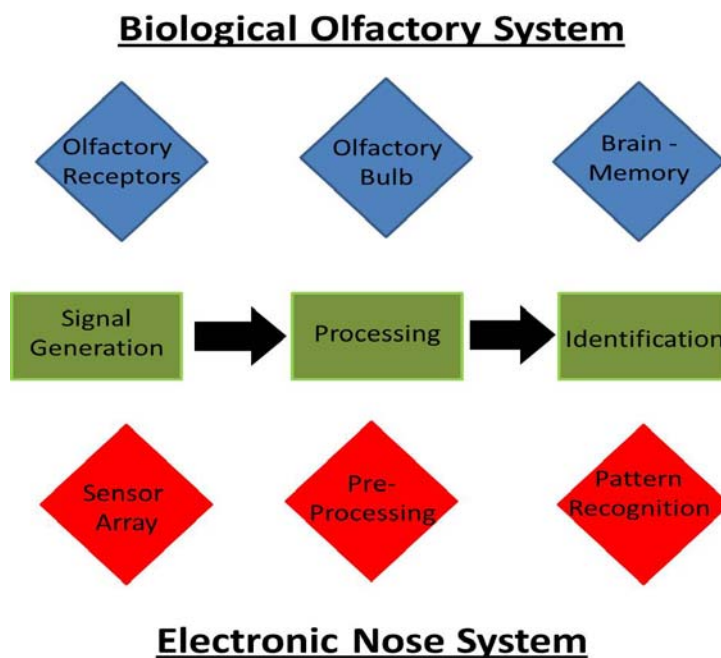
Figure 1.1 Comparison of a biological and electronic olfaction system.

Section 1.1 Nanomaterials for Vapor Detection

1.1.1 Nanomaterial Advantages

Recent advancements in nanofabrication have provided the potential for effective

and inexpensive methods of mimicking the olfaction system. A primary advantage of

nanomaterials in the fabrication of sensor elements is their high surface area-to-volume

ratios. A high surface area-to-volume ratio implies that interactions which take place on

a material's surface have substantial influence over properties of the bulk material. This

unique characteristic provides a means for establishing a direct correspondence between

properties of the nanostructures and the composition of the medium in which the

nanostructure is immersed.

To date, a variety of nanostructures have been employed as gas sensing elements,

such as: carbon nanotubes, Metal Oxide Semiconductor (MOS) nanowires, thin films,

metallic nanoparticles, conducting polymers, and combinations of these [1,41]. The

focus of this study is a novel nanomaterial, nanosprings, whose spiral structure yields a

material with ten times the surface area of carbon nanotubes or nanowires. The insulating

nature of the silica structure composing the nanospring prevents its use as a

conductometric sensor directly; however, it does provide a high surface area substrate for

functionalization with other gas sensitive materials [6-12].

1.1.2 Nanosprings Mats for Use as Gas Sensors

The current study employs a nanospring substrate functionalized with a thin film

of metal oxide as the primary sensing element. Metal oxide semiconductors (MOS) are

optimum candidates for gas sensing applications due to their low cost, flexibility in

production, large range of detectable gases, and simplicity of use [13-27]. A MOS coated

nanospring behaves as a chemiresistor in the presence of chemical species. A chemiresistor is a solid-state device with a conductance strongly dependent on chemical reactions at the material's surface. An example of such a device is a thin film of MOS deposited atop the insulating nanospring substrate [6-9].

At high temperatures, thermally excited electrons within the MOS layer capture and ionize atmospheric oxygen. The surface charge created by the ionosorbed oxygen changes the band structure of the film near the surface through the creation of a depletion layer with a thickness comparable to that of the film. Through this mechanism, the conductivity across the entire nanospring mat is significantly diminished (figure 1.3(a)). Further interaction of surface adsorbed oxygen with nearby chemical species may reverse or enhance this effect, producing a detectable change in resistance. The magnitude and rate at which this resistance changes produces a conductometric signal dependent upon the physiochemical properties of the interacting chemical species and nature of the MOS film [22-24].

By using a variety of functional materials to create the nanospring sensor elements, an array of signals unique to the exposed chemical may be obtained. This digital "fingerprint" for each chemical species is generated through the combined response of the sensor array. This signature is unique for each chemical species and may be identified and catalogued through the use of intelligent pattern recognition systems.
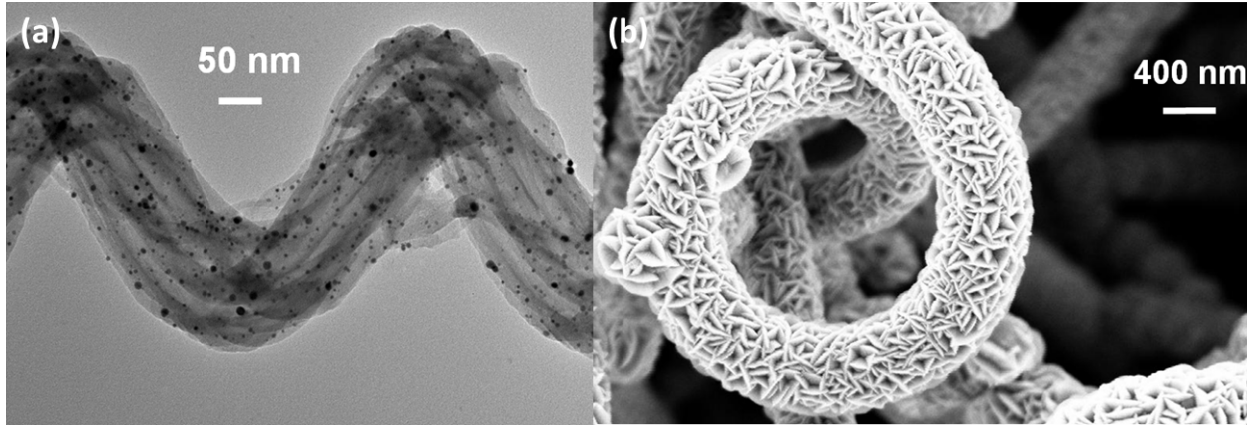
Figure 1.2 (a) TEM image of a silica nanospring, sans ZnO, coated with Pd Nanoparticles. (b) SEM image of a silica nanospring mat ALD coated with ZnO

1.2 Implementing Nanosprings as a Sensing Element

As previously discussed, the sensing elements of the present study were constructed through the deposition of a variety of gas-sensitive layers atop a mat of silica nanosprings. The functionalized mats are sandwiched between electrodes for two terminal measurements and placed atop a heater. Two types of gas-sensitive layers were studied, a polycrystalline thin film of ZnO (figure 1.2b) and a thin film of ZnO decorated by metallic nanoparticles (figure1.2a). The gas-sensing response for these elements is defined as σ_g/σ_a for reducing gases and σ_a/σ_g for oxidizing gases, where σ_a represents the conductance of the chemiresistor in air and σ_g represents chemiresistor conductance under the presence of analyte gas. For reducing gases, interaction with surface adsorbed oxygen releases trapped electrons back into the bulk; for oxidizing gases, more electrons are consumed in the reaction [27-29].
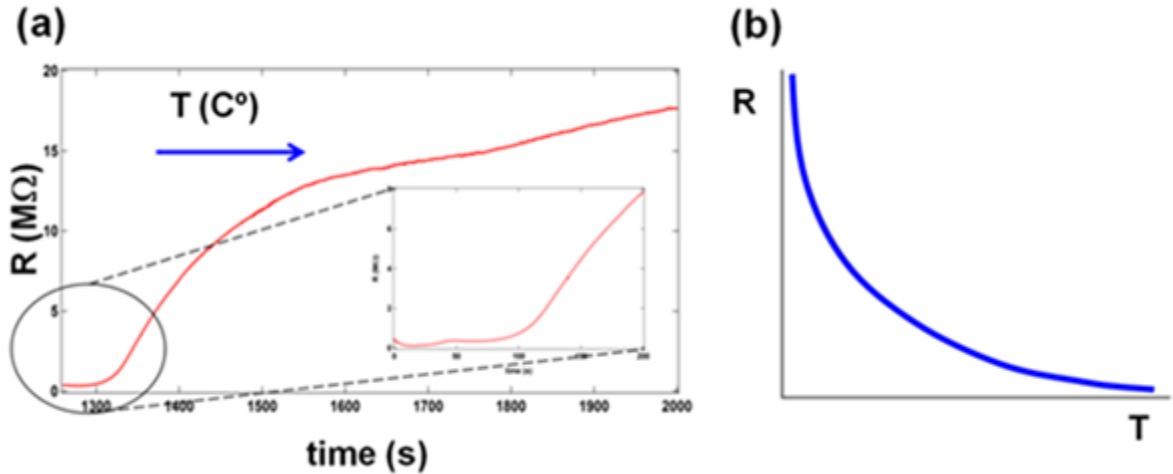
Figure 1.3 (a) heating profile of ZnO coated nanospring based chemiresistors compared with (b) typical heating profile of bulk ZnO.

1.2.1 Polycrystalline ZnO

As discussed in section 1.1.2, the primary mechanism for gas sensor response is the trapping of electrons by adsorbed molecules and the subsequent band bending induced by these charged species. For a polycrystalline layer of ZnO, adsorption of oxygen molecules at the surface extracts electrons from the conduction band and traps them at the surface to form ions, thereby decreasing the number of electrons available for conduction. Furthermore, the formation of ions at the surface creates a surface charge, inducing a potential gradient into the bulk and creating a depletion layer with a depth proportional to the Debye length required for the electrostatic screening of these charges. The atomic form of oxygen, O^- , is the dominate form of oxygen at the temperatures required by sensing (~400 ^{o}C) [22]. Adsorption of these oxygen ions occurs on the surface of individual grains creating a depletion layer and surface charge within each grain. The contact of adjoining charged surfaces within the ZnO layer forms a Schottky barrier between individual grains and hence a further increase in bulk resistance [14-18].

Upon reaction with analyte gases, surface O⁻ is consumed through the redox reaction and releases trapped electrons back into the bulk, increasing the number of electrons available for conduction while simultaneously decreasing the magnitude of the surface charge. Together, these effects create a substantial decrease in the depth of the depletion regions and hence a lowering of the Schottky barrier between grains [23,24]. Provided that these changes in depletion depth are comparable with the film's thickness, they can be observed macroscopically as a change in bulk conductivity.
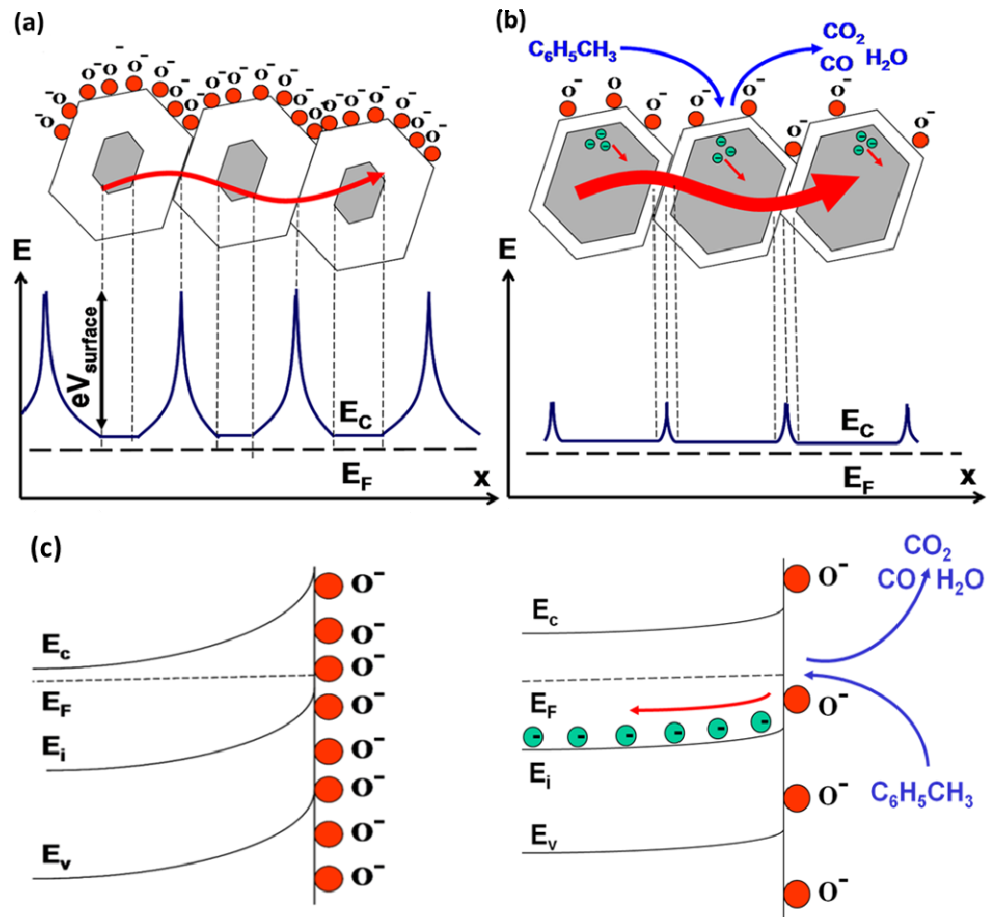
Figure 1.4 Energy level diagram of polycrystalline ZnO (a) under the presence of synthetic atmosphere (b) after exposure and subsequent oxidation of toluene. (c) The corresponding band structure near the surface of the grain for both conditions

For a polycrystalline layer of ZnO, the sensitivity may be enhanced or degraded by modifying the deposition parameters of the film. The primary deposition parameter influencing gas-sensing response is the average diameter of the individual metal oxide grains. This property of the ZnO coating affects the degree to which changes in the depletion layer influence conductivity across the bulk – this degree of change may be regarded as the sensitivity of the sensor element [17-19]. Grain size may be controlled through Atomic Layer Deposition (ALD) processing parameters. A study was performed to determine the optimal ALD parameters for maximum sensitivity of the nanospring sensing element.

In the case of polycrystalline ZnO, individual grains on the nanospring surface may be divided into two regions whose sum accounts for the overall conductance. The first is a bulk region with conductivity uninhibited by adsorbed chemical species; the second is a surface region with conductivity strongly dependent on the depth of the depletion region formed by adsorbed chemical species [13, 23-24]. A schematic of this effect can be seen in figure 1.4. In this case, the energy required for an electron to be in the conduction band is a function of depth, z.

The depth of the depletion layer may be calculated using the Poisson equation and the case for electroneutrality. Boundary conditions for the Poisson equation are obtained from the fact that the potential gradient induced by adsorbed species stops upon reaching the depletion depth. Also, past this depletion depth, the band structure of the material returns to normal and the energy required for conduction is the same as the energy required for conduction through the bulk material, E_C. These conditions yield a solution for Poisson in the following form:

$$E(z) = E_c + \frac{e^2 \cdot n_b}{2 \cdot \varepsilon \cdot \varepsilon_0} \cdot (z - z_d)^2, \text{ where}$$

E(z) denotes the energy required for conduction at a depth z, z_d denotes the depletion depth, n_b the bulk electron density, and e the carrier charge.

This relation provides a model for the magnitude of band bending in E_c displayed in figure 1.4c, and hence a means for calculating surface charge. The potential induced at the surface, V_S, may be found using the relation $V = \frac{E}{q}$, and an expression for the number of charge carriers capable of conduction near the surface, n_s, may be found as a function of the surface charge:

$$n_S = n_b \exp\left(-\frac{e \cdot V_S}{k_B \cdot T}\right), \text{ where}$$

k_B is the Boltzmann constant, T the temperature in Kelvin, e the electron charge, and n_b the bulk electron density.

Conductance through the entire sensing element is a function of both n_s and n_b, and the sensitivity of the element is proportional to the ratio $\frac{n_S}{n_b}$. These conclusions imply that bulk conductance is strongly dependent on the surface potential for grains with a thickness comparable to the induced depletion depth. This surface potential is dependent on the concentration of ionosorbed oxygen and its interaction with local chemical species, therefore, bulk conductivity may be regarded as dependent on local chemical species.

1.2.2 Metallic Nanoparticles

It has been previously reported in literature that thin film semiconductor gas sensors exhibit large conductance changes upon exposure to a changing atmospheric composition [13-31]. However, the magnitude and rate at which this conductance changes is similar for many different chemical species, making distinction between chemically similar molecules a major problem.

A semiconductor's electrical properties are influenced by interactions with many ambient chemical species, not just the analyte. Any molecule with the proper physiochemical properties may interact with areas of ionosorbed oxygen at the semiconductor surface. These interactions can influence the depletion depth in a nearly indistinguishable manner, making distinction between various gas molecules problematic when attempting to use a single material for sensing multiple chemicals [25-27].

A potential solution to this problem is the use of catalytic additives which promote the reaction of the desired molecule and hence provide a mechanism for selectivity. For the present study, a variety of metallic nanoparticles played the role of such catalysts. These nanoparticles were deposited atop the semiconductor coating through standard wet-casting procedures. Upon deposition of the nanoparticles on the semiconductor's surface, a Schottky barrier is formed between the metallic nanoparticle and the semiconductor layer as the Fermi levels within the two materials achieve an equilibrium state. Further modulation of this Schottky barrier can be achieved through the interaction of nearby chemical species with the deposited nanoparticles, providing a mechanism for ambient chemical species to influence bulk conductivity [8-9, 25-27].

Metallic nanoparticles interact with analyte molecules through the chemisorption field effect. This effect is a property of metallic particles that results in a change in the metal's work function upon adsorption of gases from the environment. Initially, the change in work function is caused by the formation of electric dipoles at the surface when oxygen ionosorbs to the surface. This dipole moment is enhanced or diminished by the redox reactions taking place on the surface with ambient chemical species, further modulating the required energy to remove an electron from the nanoparticle surface [25-28]. According to Schottky theory, this change in work function leads to a change in the height of the metal-semiconductor potential barrier and thus the position of the Fermi energy level at the surface of the semiconductor. This change in Fermi energy within the semiconductor may be viewed as a change in the number of electrons available for conduction and hence as a change in conductance within the semiconductor.

Functionalization of the semiconductor surface with metallic nanoparticles not only provides a mechanism for selectivity, but has also been shown to improve sensitivity. There exist several mechanisms that contribute to this increase in sensitivity. One such mechanism is widely established and referred to as the "spillover effect" in literature [25]. This effect describes the property of metallic nanoparticles to catalytically dissociate O_2, allowing the atomic products of this reaction to diffuse into the surrounding metal oxide support. This dissociation increases the quantity of oxygen capable of repopulating vacancies at the ZnO surface created by the redox reactions with the analyte chemical species. This effect results in a net increase of the number of surface sites available for analyte interaction and a faster degree of electron transfer from the surface to the bulk due to the increased number of reactions able to occur within a smaller

timeframe compared to pristine ZnO [25-27]. An increase in the rate of electron transfer manifests itself as an increase in sensitivity because, due to the abundance of atomic oxygen within the surrounding metal oxide support, more oxidation reactions are able to occur within the same timeframe, resulting in an increase in the net charge transfer from the surface to bulk. A diagram of this effect is displayed in figure 1.5.
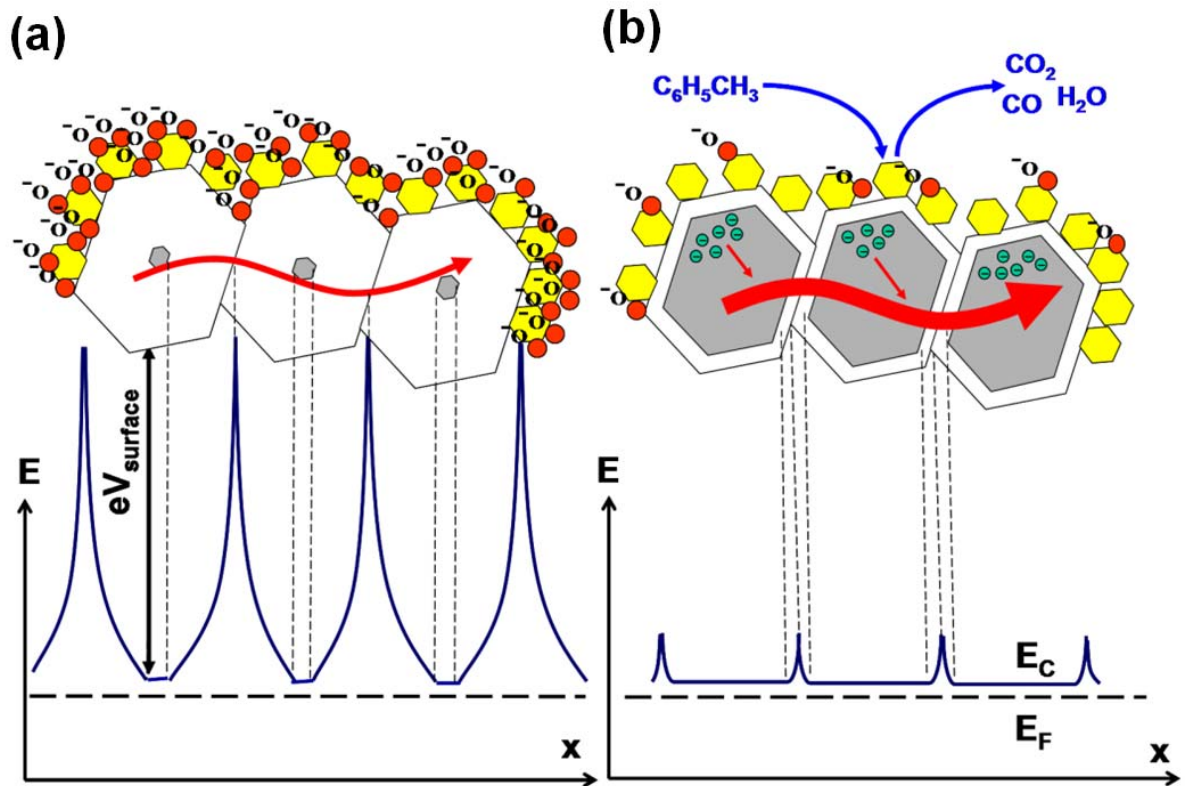
Figure 1.5 – (a) energy level diagram of ZnO nanocrystals decorated with metallic nanoparticles under normal synthetic atmosphere and (b) after exposure and subsequent oxidation of toluene.

To receive a signal from the metal nanoparticle's interaction with the target gas, charge must be transferred from the metal to the bulk semiconductor. For this to occur, charge carriers originating in the metallic nanoparticle must overcome a barrier of energy,V_s, referred to as the Schottky barrier:

$$V_s = \Phi_M - \chi_e + \Delta\mu, \text{ where}$$

Φ_M represents the work function of the metal, χ_e the semiconductor's electron affinity,

and $\Delta\mu$ the difference in chemical potential between the two materials. This statement

implies that a change in the metal's work function produces a change in the Schottky

barrier height and hence a change in the material's electronic properties.

A condition for metallic nanoparticles deposited on a semiconductor surface is

thermal equilibrium between the Fermi energies of the two materials. This restriction is

met by charge redistribution near the metal-semiconductor interface that results in band

bending at the semiconductor's surface. The standard Schottky model predicts a depletion

depth within the semiconductor material proportional to the square root of the difference

in Fermi energies: For nm sized particles, however, this is not the case as the radius of the

nanoparticles cannot be smaller than the induced depletion depth. For this reason,

Zhdanov [25] developed a more accurate description of the depletion depth z_d within a

nanoparticle at the surface of a semiconductor with the following relation:

$$z_d \cong \left(\frac{3 \cdot \varepsilon_s \cdot r_m \cdot \Delta E}{2\pi \cdot e^2 \cdot N_d}\right)^{1/3}, \text{ where}$$

N_d represents the concentration of charge donors in the semiconductor, ΔE the difference

of Fermi energies between the metal and semiconductor, ε_s the semiconductor dielectric

constant, e the electron charge, and r_m the radius of the metallic nanoparticle. This

model works well for nanoparticles with a diameter less than the depletion depth.

Regardless of the approximation used, however, it is evident that a change in the Fermi

levels is directly proportional to a change in the depletion depth; and by this mechanism,

metallic nanoparticles deposited on a semiconductor's surface may be used as gas sensors.

1.3 Optical Excitation

There are many problems inherit with thermally activated sensing elements, such as: increased power consumption, degradation of sensor elements and contacts, enlarged size of device, and increased level of noise. For these reasons, it is desirable to use a sensing element that is active at room temperature. For the present study, optical excitation was investigated as a potential mechanism for room temperature sensitivity.

ZnO, with a band gap of 3.4 eV, is well known for its high optical activity [28-31]. Upon exposure to UV light with energy equal to or greater than 3.4 eV, high energy electron-hole pairs are generated within the ZnO layer. The holes migrate to the surface of the ZnO layer and discharge adsorbed oxygen ions, inducing a decrease in the width of the depletion layer. The resulting unpaired electrons continuously accumulate within the material until the desorption and adsorption of oxygen reaches an equilibrium state [28-29].

Therefore, illumination by UV light causes a net increase in conductance along with an increase in the concentration of high energy electrons. These high energy electrons are capable of ionizing atmospheric oxygen with a higher energy, leading to a dominant coverage of oxygen in the atomic form opposed to the molecular form which exists under normal conditions at room temperature. Atomic oxygen is known to be more chemically reactive than its molecular counterpart, allowing for a quicker oxidation of analyte species and hence an increase in the amount of charge transferred per unit time

which manifests as an increase in sensitivity. A schematic of thermal vs. optical

excitation is displayed in figure 1.6.
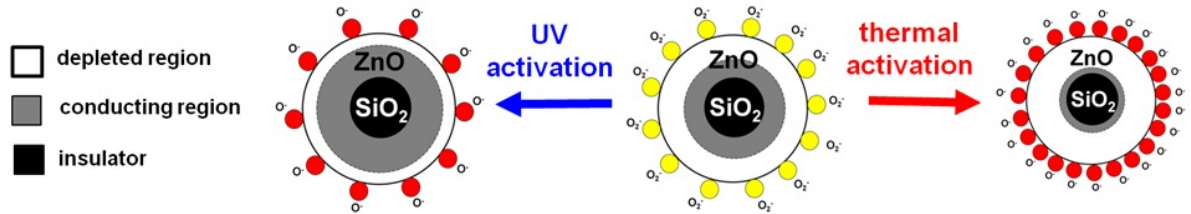
Figure 1.6 UV activation of ZnO coated nanosprings. Upon exposure to UV, molecular
oxygen desorbs from the surface and high energy electrons capture and ionize atomic
oxygen.

Optical excitation of the nanospring element not only provides a mechanism for

room temperature sensitivity but also a mechanism for drastically reducing the refresh

time of the sensing elements. The refresh time of a sensing element refers to the time

required for complete oxidation of the analyte species and the subsequent restoration of

surface coverage by ambient oxygen species. For gases with a one-step catalytic

oxidation reaction, such as CO, the recovery rate is greater when compared to analytes

which involve several intermediate oxidation stages, such as complex organic molecules.

Analytes with complex structures generate intermediate reaction products that remain

attached to surface defects and oxidize at a slower rate, causing an increase in the amount

of time required to restore oxygen coverage.

For the sensing of such complex molecules, it is desirable to decrease the recovery

rate in order to achieve improved accuracy and efficiency when performing multiple

exposures in a short duration – as is the nature of gas sensing in a real life environment.

One mechanism for reducing recovery rate in this situation is exposure to UV light after

the initial sensing reaction has taken place. It is widely established that partial oxidation products of many chemicals may be dissociated by UV light. These dissociated oxidation products are more readily oxidized by surface oxygen; hence, post exposure to UV light provides a mechanism for reducing the recovery rate of the nanospring sensing element [29-30].

1.4 Chemical Pattern Analysis

Pattern Analysis is a critical building block in the production of gas sensing devices which utilize a variety of functional materials to generate conductometric signals upon exposure to analyte species. The successful design of a pattern recognition system for machine olfaction requires a careful consideration of all the parameters involved in processing the multivariate data. To date, a number of different methods from statistical pattern recognition, machine learning, and neural networks have successfully classified chemicals based on their electronic nose signatures [32-36]. In this study, an analysis of methods commonly used for processing MOS sensor data was performed. These algorithms were tested using data from the nanospring sensor array to demonstrate the ability of the sensor to distinguish between chemically similar molecules.

1.4.1 Feature Extraction

The effect of surface redox reactions on bulk conductivity has been observed in the current study and a response curve typical of the nanospring element is displayed in figure 1.5. In order to use such a response curve in a pattern classification system, various scalar features of the signal must be extracted in a pre-processing phase known as feature extraction. The features that are chosen in this phase must sufficiently describe the signal and are themselves a subject of research. The most common features used for pattern

16

recognition and classification include: time of absorption, time of desorption, area under absorption curve, area under desorption curve, and maximum amplitude of response [32-33]. The present study is intended to demonstrate the feasibility of the nanospring sensor element to detect explosives; therefore, response time is a primary factor to consider when performing feature selection. Features regarding the adsorption of the analyte on the sample were the primary features studied, and supporting evidence indicates that these features also provide maximum discrimination. The adsorption features studied included: area under the absorption curve, time of adsorption, and the rate parameter of an exponential function fit to the absorption curve. Once extracted, these features formed a feature vector, x, which became the input to the various pattern recognition algorithms capable of performing classification.
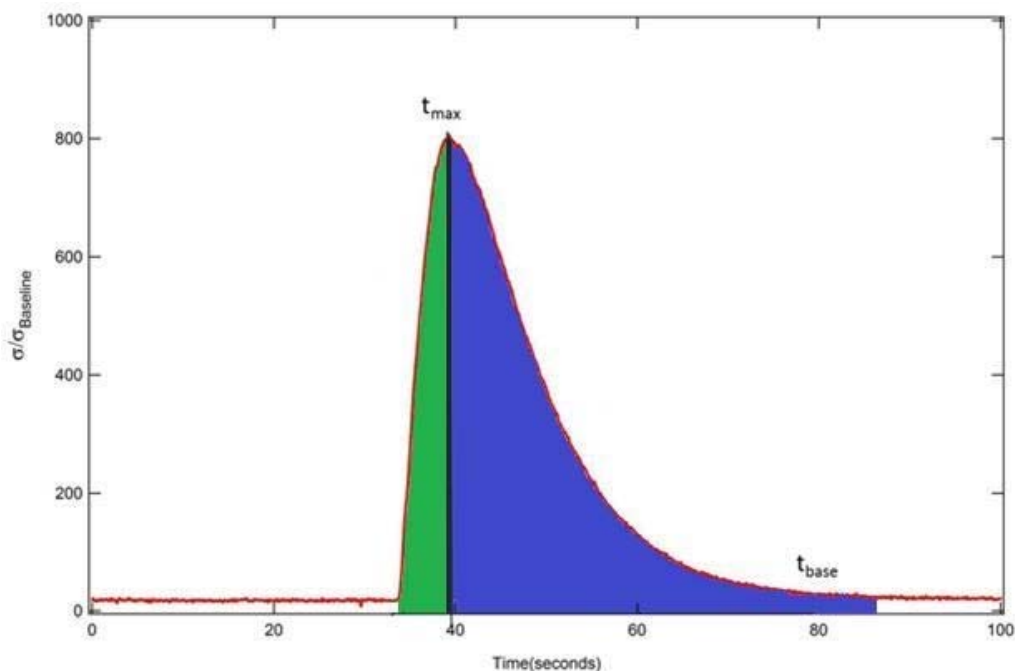
Figure 1.7 Response of Pd NPs to Acetone. The common features extracted are area under absorption curve (left region), area under desorption curve (right region), time to maximum response, and time to baseline return.

1.4.2 Pre-Processing

When using an array of sensors to generate feature vectors, high-dimensional input data results with a dimensionality equal to or greater than the number of sensors in the array. The cost of processing such data is high, and the problem of increased data complexity with an increasing number of sensor elements is commonly referred to as "the curse of dimensionality" [32-36]. The purpose of a pre-processing algorithm is to mitigate this problem by finding a low-dimensional mapping from the original input vector that preserves most of the discriminatory information. The most basic pre-processing projection multiplies a feature vector, x, by a weight vector, w, and uses the projected data as inputs for the classification algorithm:

$$y = w^T x, \text{ where}$$

y is the projected feature, w the weight vector, and x the original input feature vector. The number of dimensions in the data may be reduced by selectively choosing the dimensions of the weight vector. The two most common pre-processing algorithms for dimensionality reduction in processing electronic nose data are principal component analysis (PCA) and linear discriminant analysis (LDA) [1, 32-36]. PCA seeks to transform the input features by means of a projection along the distance of maximum variance. In this method, separation, rather than classification is the primary goal. PCA is commonly used to demonstrate a sensor's ability to distinguish between chemicals through the use of a projection which maintains the variance of the data while simultaneously reducing its dimensionality [33].

LDA, on the other hand, is a method which selects a transformation vector, w, that maximizes the distance between projected class means, defined as between-class

scatter, and minimizes the distance between projected points of the same class, defined as within-class scatter. If the distribution of projected points from the same class is modeled as a probability distribution, then the transformation $w^T x$, may be described as minimizing within class variance while maximizing between class distances. For this reason, LDA is known as a signal classification technique which directly maximizes class separation. The transformation vector in LDA is referred to as Fisher's linear discriminant, $J(w)$, and is defined as the projection which maximizes the ratio of between class scatter to within class scatter [1]:

$$J(w) = \frac{w S_B w^T}{w S_W w^T}, \text{ where}$$

S_B represents the between-class scatter, S_W the within-class scatter, and w the optimal transformation vector. To find the maximum of J(w), standard techniques may be used (i.e. equate the derivative of J(w) with respect to w to 0 and solve for w). The eigenvectors of this matrix, J, form basis vectors which span the projected feature space. The degree to which the eigenvectors transform the projected data may be gauged by the corresponding eigenvalues. By selecting only the eigenvectors with the largest eigenvalues to compose the transformation vector, a reduction in the dimensionality of the data may be obtained. For this reason, LDA is also referred to as a dimensionality reduction technique [32]. An example of LDA maximizing separation between two classes may be seen in figure 1.6.
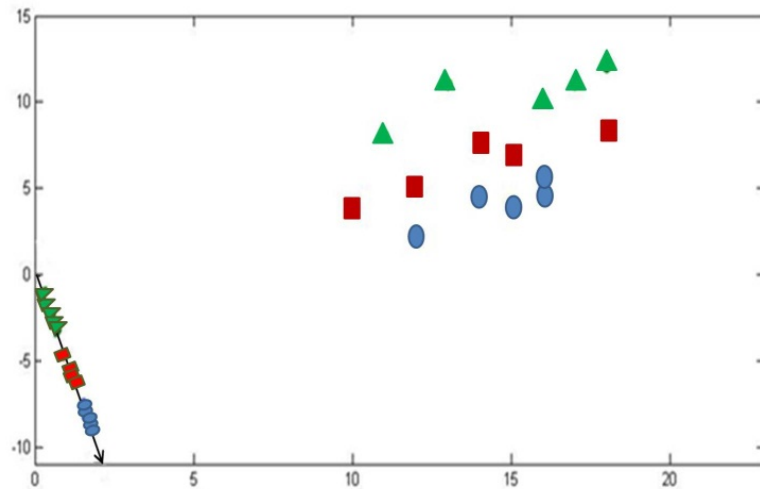
Figure 1.8 An example of Linear Discriminant Analysis performed on a test data set. The clusters of points are projected onto an eigenvector of Fisher's Linear Discriminant which allow for distinct regions among the different classes.

1.4.3 Minimum Distance Classifier

After separation between classes has been achieved, the transformation vector used to achieve separation may be applied to new input features, and the probability that an input feature vector belongs to any of the classes may be calculated within this transformation space. This probability may be calculated a number of ways, each method corresponding to a different classification algorithm. Perhaps the most intuitive of all classifier is the minimum distance classifier. In a minimum distance classifier, an input feature is classified by comparing the distance between the feature's projected value and the various class means. This distance may be calculated using the standard Euclidian metric, or, in any number of dimensions using an extension of Euclidean distance, the Mahalanobis distance: For an input feature x and a class i with mean μ_i and covariance

$\sum_i$, the Mahalanobis distance, D_i, between the input feature and class is calculated as follows:

$$D_i = \sqrt{(x - \mu_i)^T \sum_i^{-1}(x - \mu_i)}$$

An unknown sample may then be classified as the class with the least Mahalanobis or Euclidean distance to the projected feature.

1.4.4 K-Nearest Neighbor

An extension of the minimum distance classifier is the K nearest neighbor (kNN) classification algorithm. kNN classifies an input by locating the nearest k examples from the training set and selecting the predominant class within that subset. For the two dimensional LDA space studied, both Euclidean and Mahalanobis distance metrics gauged the distances between the sample projection and its nearest neighbors. In this scheme, kNN is capable of generating highly nonlinear classification regions effectively with small training sets. While useful for small training sets, kNN has serious limitations when dealing with large sets due to the immense storage requirements for the class data sets and the computational cost associated with computing distances to every training example [32]. In the preceding and future classification algorithms, only class means and covariances must be stored to effectively generate classification regions. These methods are more effective when dealing with large data sets.

1.4.5 Baye's Theorem

In a classification algorithm, the probability that an input feature vector, x, belongs to a class, C_i, is referred to as the posterior probability and denoted $P(C_i|x)$. In practice, the posterior probability is difficult to obtain directly and is instead calculated through the use of Baye's theorem. Baye's theorem provides a relation between the posterior probability and the probability that a given class generates the observed features, referred to as the prior probability, $P(x|C_i)$. Baye's theorem is stated as follows:

$$P(C_i|x) = \frac{P(x|C_i) \cdot P(C_i)}{p(x)}, \text{ where}$$

$p(x)$ is the probability density function (pdf) of the input feature x, and $P(C_i)$ the a-priori probability, that is, the probability of obtaining class i without using information from the feature vector. If all classes are equally likely, as is the case for this and many gas sensing applications, then all a priori probabilities will be of magnitude 1/N, where N represents the total number of possible classes. Moreover, because the input feature has probability unity and is the same for all classes, it may be omitted from the posterior probability calculation. Therefore, only the prior probability must be calculated, $P(x|C_i)$, for this particular application.

1.4.6 Multivariate Gaussian Discriminant Analysis

One of the most common probability density functions encountered in practice is the Gaussian (or 'Normal') distribution. The Gaussian distribution is commonly used as a model for physical systems because of its computational tractability and common occurrence in real world observations [1, 32-36]. By assuming the pdf of an *l-*

dimensional feature vector x belongs to a class C_i follows a Gaussian distribution, the

prior probability, $P(x|C_i)$ may be calculated as follows:

$$P(x|C_i) = \frac{1}{(2\pi)^{l/2}|\Sigma_i|^{l/2}} \exp\left(-\frac{1}{2}(x - \mu_i)^T \Sigma_i^{-1}(x - \mu_i)\right), \text{ where}$$

μ_i denotes the mean of a class i and Σ_i the $l \times l$ covariance matrix. Both the mean and

covariance of a class are obtained from the training data. With a well-defined pdf, a

discriminant function can be built using $P(x|C_i)$ that outputs a value capable of

determining which class an unknown input feature vector belongs to. Due to the

monotonic nature of the Gaussian pdf and the presence of the exponential, it is simplest

to deal with a discriminant function that incorporates Baye's theorem and the natural

logarithm of the density function:

$$g_i(x) = -\frac{1}{2}(x - \mu_i)^T \Sigma_i^{-1}(x - \mu_i) + \ln P(C_i) - \frac{1}{2}\ln(2\pi) - \frac{1}{2}ln|\Sigma_i|$$

With a discriminant function of this nature, the function output is directly proportional to

the probability that the input feature belongs to class i. Decision boundaries are formed

along the points at which the probability that an input feature belongs to two classes, i,j,

is equal.

Chapter 2: Experimental Design

Data for the project was obtained through conductometric sensing of nanospring elements under varying atmospheric conditions. The sensing elements studied were 1cm x 1cm silica substrates coated with mats of functionalized nanosprings, shown here in figure 3.1. Due to the high temperatures required for sensing, mechanical connections proved to be the only reliable method of obtaining electrical measurements under the conditions required. During data acquisition, nanospring mats were positioned on ceramic platforms and secured in place using stainless steel contacts mechanically compressed into the sample material to form an ohmic contact. The ohmic nature of these contacts was confirmed through IV characteristic studies. Stainless steel wiring housed in a ceramic casing connected the two terminal testing systems to their respective source/measure units. To perform sensing on high concentrations of explosive materials, the sensing elements were placed into a tube furnace for both temperature and atmosphere control. Under these conditions, data from eight sensors was gathered simultaneously by sourcing voltage and measuring the corresponding current within the samples. For testing to high explosive molecules, substantially smaller concentrations of the analyte material were required. For these tests, the sensing elements were placed directly in front of a prototype instrument, the VaporJet, which produced extremely small concentrations of vapor at its outlet. Under these conditions, data was gathered in a similar manner but using only one sensor at a time. The two testing systems just described may be seen below in figures 2.3 and 2.4.
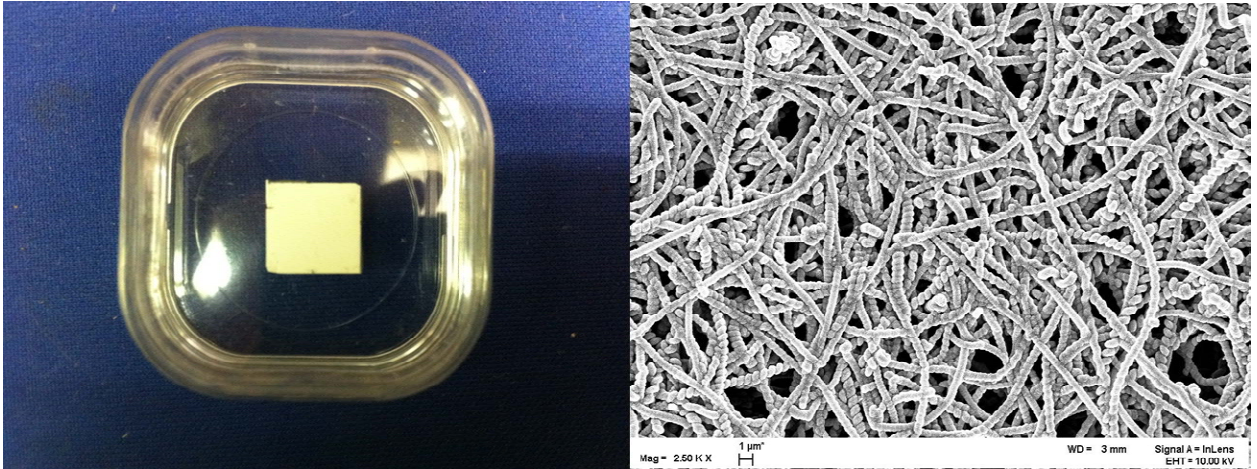
Figure 2.1 A mat of nanosprings (right) grown atop a 1cm x 1cm silica substrate (left).

2.1 Sample Characterization

Nanospring mats were grown using a vapor-liquid-solid (VLS) technique in a furnace

operated at atmospheric pressure. A detailed description of this process has been reported

by Wang et al. [11] and McIlroy et al. [10]. The process uses a gold layer atop a Si

substrate as a catalyst which is exposed to a proprietary silicon precursor as well as a

constant O_2 flow rate for the VLS parameters. Under these conditions, the growth time for

~80 μm thick nanosprings mats is approximately 15 minutes. A thin film of ZnO material

was applied to the mats using the Atomic Layer Deposition (ALD) technique. ALD

utilizes a two-step reaction sequence of self-saturating chemical reactions between

gaseous precursor molecules and the solid surface to deposit films in a monolayer-by-

monolayer fashion. The ALD coating of ZnO was achieved in a tube furnace heated to

170 ^{o}C using diethyl zinc and water as the precursors and N_2 to purge the system between

cycles [44]. The ZnO layer thickness is controlled by the number of cycles used during

ALD as well as the precursor and purge pulse widths. Using the above ALD parameters

for 200 cycles, a uniform nanocrystalline ZnO layer was obtained with an average crystal size of approximately 10nm and a layer thickness of approximately 30nm (figure 1.2b).

The crystal structure of the ZnO nanocrystals was verified using standard X-ray diffraction (XRD) techniques. Displayed in Figure 2.1 is a representative 2θ-XRD rocking curve for the ZnO coated nanospring sample. The primary peaks of ZnO are all present and indicated by the red bars, while those of Au are represented by the blue bars (Au is the catalyst used for nanospring synthesis). The peaks with an asterisk are merely artifacts of the hotspots within the x-ray detector. Below is an XRD spectrum of a sample of ZnO coated nanosprings. This spectrum is indicative of a high quality ZnO coating.
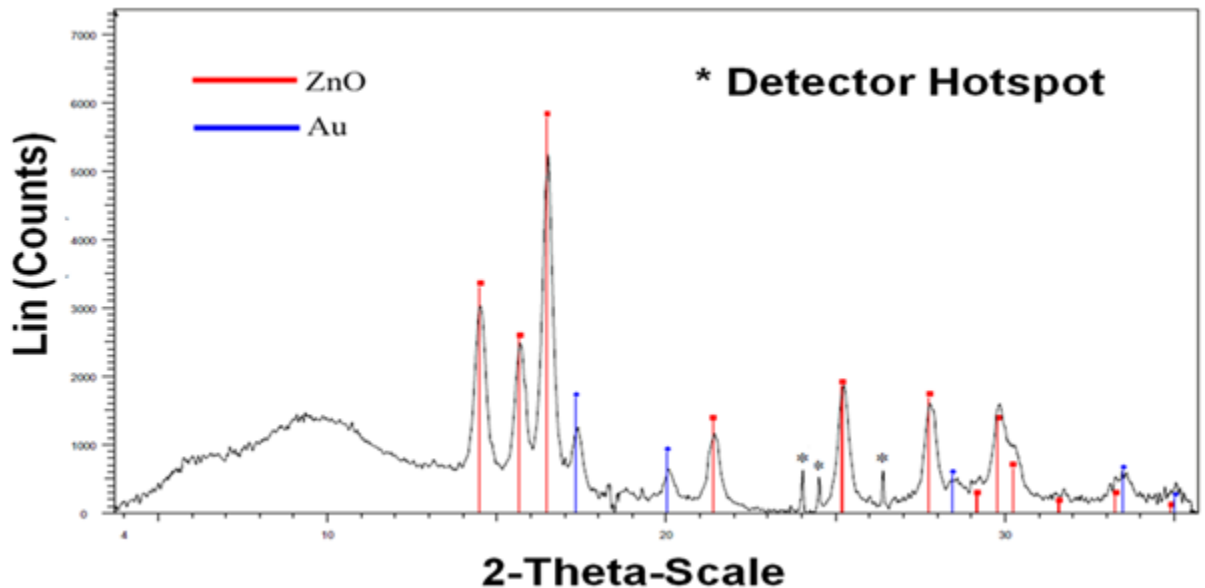

Figure 2.2 - 2θ-XRD rocking curve for ZnO coated nanosprings.

Metallic nanoparticles were deposited atop the ZnO coated nanosprings by dipping the nanospring sample into a solution containing the desired nanoparticle and then left to dry at room temperature for evaporation of the solvent. The sample was then

placed into an atmosphere of H_2 for 15 minutes at 500 ^{0}C and then cooled to room temperature in an N_2 atmosphere to avoid oxidation of the nanoparticles. This technique produced a particle size distribution between 2-5nm with an average size of 2.4 ± 1.3nm.

2.2 Experimental Design

Gas sensing data for the nanospring elements was obtained conductometrically with the use of a voltage source, ammeter, and computer for LabView assisted data acquisition. An NI CompactDAQ 9178 chassis was used in conjunction with an NI 9264 voltage source and NI 9203 ammeter to perform the required measurements. 10 Volts were applied to the system using the NI 9264 and corresponding current measurements were taken from each sensor using the NI 9203 at a rate of 10 samples per second. These measurements were obtained simultaneously for eight sensors when performing data acquisition to explosive simulants and multiplexed when obtaining data for the sensing element's limit of detection to high explosives.

2.2.1 Building the Pattern Recognition Library

The three explosive simulants tested were Acetone, Ethanol, and Toluene. Toluene is both itself an explosive molecule and a degradation product of many common explosives, such as TNT. Acetone, also an explosive molecule, is a common degradation product of TATP, a common material used in the manufacture of IEDs. Ethanol possesses the necessary hydrogen and oxygen groups to be considered explosive. An MTI OTF-1200x quartz tube furnace was used as a controllable atmospheric chamber for all testing of the sensing elements to the explosive simulants and degradation products. The atmospheric chamber required only two connections, an inlet and exhaust. At the inlet, a Swagelok tee element connected the tube furnace to the gas mixing system

27

through ¼" Teflon tubing. A constant flow of synthetic atmosphere (UHP Air supplied

by AirGas) was maintained into the furnace at all times and analyte gas species were

introduced to the flow via a standard bubbler. The outlet of the bubbler was connected to

a valve at the tee element between the cylinder of UHP air and tube furnace inlet.

Injections of analyte species were performed by switching between pure synthetic air and

the same synthetic air passed through a bubbler with a headspace containing a known

concentration of the analyte. A schematic of this design is depicted in figure 2.3. During

baseline acquisition, valve 1 remained closed and 2 open. During exposure valve 2

remained close and valve 1 was opened. Typical exposure times were ~5 sec. At the

exhaust port, an ULVAC GLD-040 vacuum system provided the necessary negative

pressure to maintain a constant flow rate through the tube furnace. Flow rate was

monitored using an Omega Fl-1803 Air Rotameter.
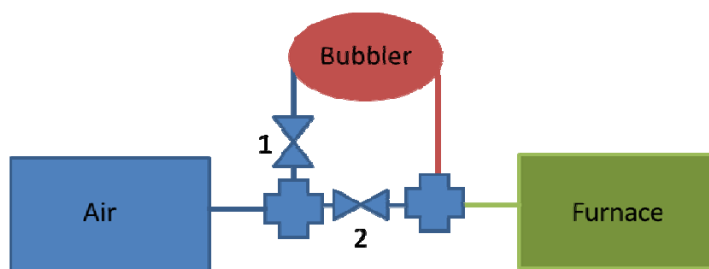
Figure 2.3 Experimental design for explosive simulant and degradation product
testing.

Sensing elements were placed onto a ceramic platform and inserted into the tube

furnace heated to a temperature of 400 ^{0}C until a steady-state baseline was observed. A

steady state baseline, within the context of nanospring sensing elements, occurs when

thermal generation of carriers and the ionosorbtion of oxygen species achieve an

equilibrium state. This typically occurred within 10 minutes of reaching operational

temperature. With the above experimental design, various concentrations of the explosive

simulants and degradation products were produced by varying the concentration of
analyte within the bubbler and the duration of exposure. A picture of the testing system
used is displayed in figure 2.4.
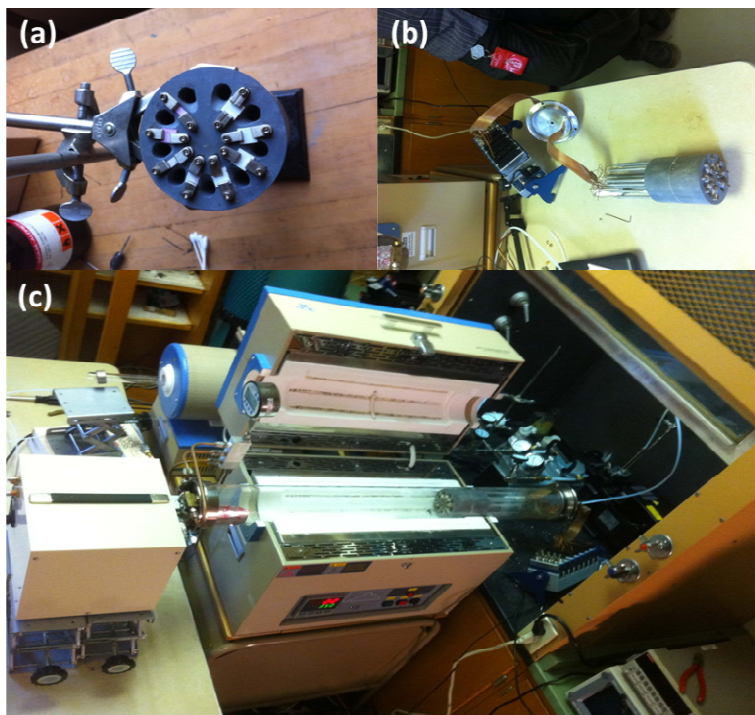
Figure 2.4 (a) the sensing platform (b) connected to the NICompactDAQ9178 and (c)
placed in the environmental chamber.

2.2.2 Limits of Detection for High Explosives

For determining limits of detection to high explosives, direct exposure to the
explosive chemical was required. Due to the volatile nature and purchasing restraints
inherit to these types of explosive materials; a separate instrument was required to
generate the necessary concentrations of explosive vapors. MicroFab's VaporJet system
allowed commercially available explosives to be exposed to the sensing elements in parts
per billion (ppb) concentrations [45]. Explosives were obtained in the form of small
concentrations diluted in solvent from AccuStandard inc. For TNT, a concentration of 1

mg/mL was diluted in a (1:1) AcCN:MeOH solvent. For TATP, a concentration of 0.1 mg/mL was diluted in an AcCN solvent.

Explosives dissolved in solvent were placed inside a capillary tube and subjected to pressure pulses by a piezoelectric material surrounding the tube. Pressure pulses from the piezoelectric material caused droplets of varying size to be ejected from the tube end. Different concentrations of explosives were obtained by varying the AC signal sent to the piezoelectric material. The explosive-containing solvent was deposited from the VaporJet's capillary tube onto a platinum RTD under a constant flow of 10 sccm of synthetic atmosphere (UHP Air supplied by AirGas). The RTD was heated using a two-step cycle to expose the sensing elements to the desired concentration. The first temperature in the cycle evaporated only the solvent, allowing the explosive material to remain on the heating element; the second step temperature then evaporated the remaining explosive material, introducing the vapor to the flow and hence the nanosprings sample.

To keep the concentration of explosive molecules reaching the sample as precise as possible, sensor elements were placed directly in front of the VaporJet exhaust, and the concentration at the instrument's outlet was assumed to be the concentration reaching the sample. A soldering iron, Weller SPG-80L, provided the necessary thermal energy to the sample which was placed directly atop the heated iron tip. An aluminum casing surrounding the soldering iron allowed ceramic screws and washers to secure the sample atop the heating element by applying pressure to two gold coated stainless steel contacts embedded in the sample (figure 2.5a). Standard sputtering techniques were used to coat the steel contact with gold in an effort to prevent oxidation of the contacts at high

temperatures. A picture of the experimental design for limit of detection measurements is shown below in figure 2.5.
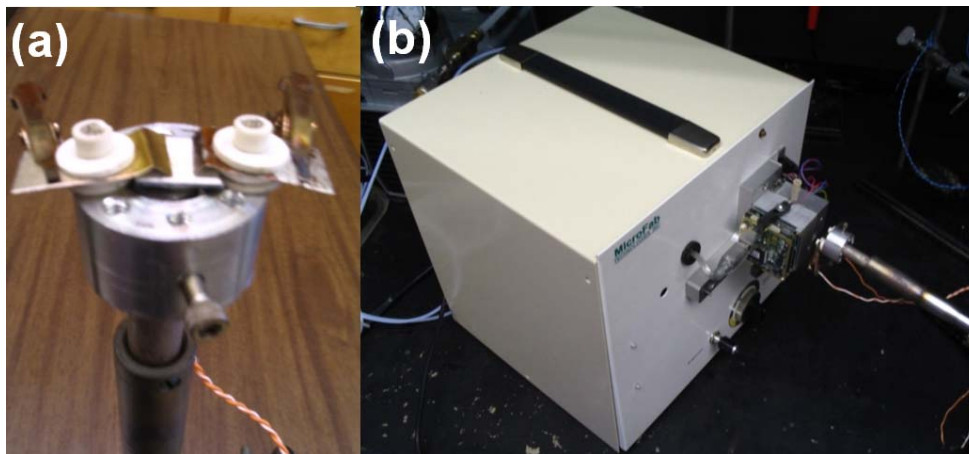
Figure 2.5 (a) the sensing element connected the heating element and (b) exposed to explosive vapors through the VaporJet system.

2.2.3 Room Temperature UV Studies

For performing gas sensing studies under UV light, a similar design to figure 2.4 was implemented. Sensor elements were irradiated by a 3W 385nm LED light source from S-Bend Technology Ltd. and placed into a flow of UHP air supplied by Airgas. A standard bubbler exposed the illuminated sensor elements to concentrations of analyte vapor in the range of 500 ppm in a similar manner to figure 2.4. A PVC top was embedded with the LED elements and connected to a gas inlet at its center. A loose fitting of the top over the sensing platform allowed airflow to be maintained in a vertical fashion with the exhausted gas exiting the sides of the sensing platform. A schematic of this design is displayed in figure 2.6

Figure 2.6 Design of the UV testing system. The same sensor platform from figure 2.4a was exposed to UV and a constant flow of variable atmosphere.

Chapter 3: Results

3.1 Polycrystalline ZnO

During testing, nanospring sensing elements were heated to a temperature of 400 ^{o}C in synthetic air at atmospheric pressure to obtain an initial steady state resistance. An example of a response typical of the ZnO coated nanospring sensor to an acetone pulse of ~ 500 ppm is displayed in figure 3.1 (a), (b). For ZnO nanocrystals with an average diameter of 8nm (figure 3.1(a)), a resistance change from a few MΩ to a few kΩ was obtained. For an average size of 15nm (figure 3.1(b)), a resistance change from tens of MΩ to a few kΩ was obtained. This variance in the magnitude of response is a characteristic of the length scale of the ZnO coating. A diagram of conductance change upon heating and subsequent exposure to Acetone can be seen in figure 3.1(c) as a function of average grain size.

For bulk ZnO, the addition of thermal energy to the system excites free carriers into the conduction band, creating a drop in the material's resistance. However, for thin film ZnO coated nanosprings, two competing processes are observed: (1) thermal generation of free carriers (decreasing the resistance) and (2) trapping of free electrons by the ionosorbtion of oxygen at the surface (increasing the resistance). The heating profile of figure 1.3 demonstrates that at high temperatures, the depletion layer formed by adsorbed oxygen has a substantially greater influence over bulk conductivity than does the thermal generation of free carriers. This effect is a necessary condition to achieve high sensitivity in a sensing scheme which uses the rapid catalytic reactions of analyte species with surface oxygen as the sensing mechanism.

(a) ZnO average grain size ~ 8 nm

(b) ZnO average grain size ~ 15 nm

(c)
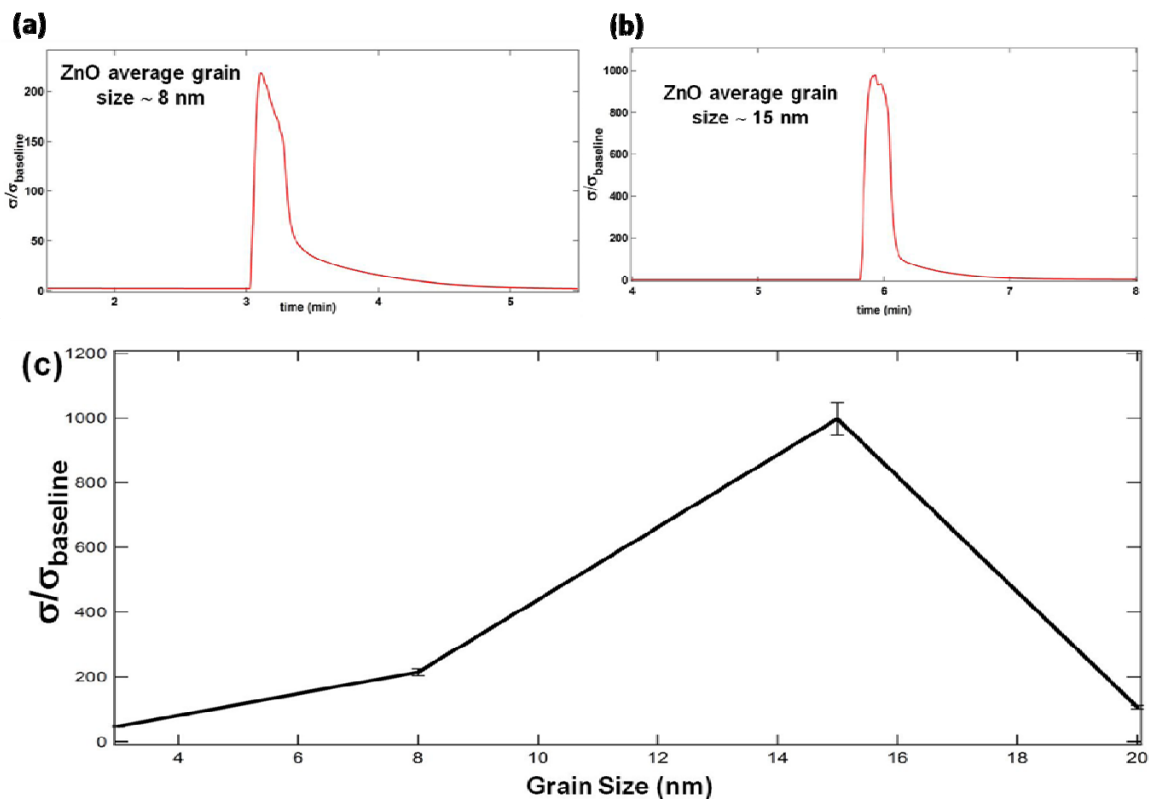
Figure 3.1 Conductance change upon heating and exposure to ~ 200 ppm toluene for a ZnO coating with average grain size (a) 8 nm and (b) 15 nm. Change in conductance as a function of grain size is displayed in (c).

Experimental real-time resistance scans as a function of ~ 200 ppm toluene, ethanol, and acetone exposures for the optimal ZnO coating is displayed in figure 3.2. For bare ZnO coated sensors with the optimum grain size of 15 nm, a relative increase in conductance by a factor of 4 was observed for toluene, 200 for ethanol, and 500 for acetone. Upon terminating the introduction of analyte species into the flow of artificial atmosphere (approximately 20% O_2 and 80% N_2), all of the chemiresistors self-refreshed and reproducibly returned to their original baselines in approximately 90s.

3.2 Metallic Nanoparticles

The addition of metal nanoparticles onto the ZnO coated nanosprings increased room temperature resistance significantly. As an example, the addition of Cu nanoparticles onto a ZnO coated nanospring increased the resistance from tens of MΩ to 10GΩ due to the formation of the aforementioned nanoscale metal-semiconductor Schottky contacts at the metal NP-ZnO interface. At a temperature of 400 ^{o}C and under a continuous flow of synthetic atmosphere, the baseline resistance stabilized around 10 GΩ. Upon the introduction of toluene, a change in conductivity by a factor of 1200 was observed compared with the 500 times change present without Cu nanoparticles. This observation confirms the claim that functionalization with metal nanoparticles increases sensitivity [25-28]. Similar to the bare ZnO coated nanosprings, the Cu coated nanosprings sensor is self-refreshing in the presence of artificial atmosphere and returns to baseline in approximately 90s as shown below in figure 3.2.
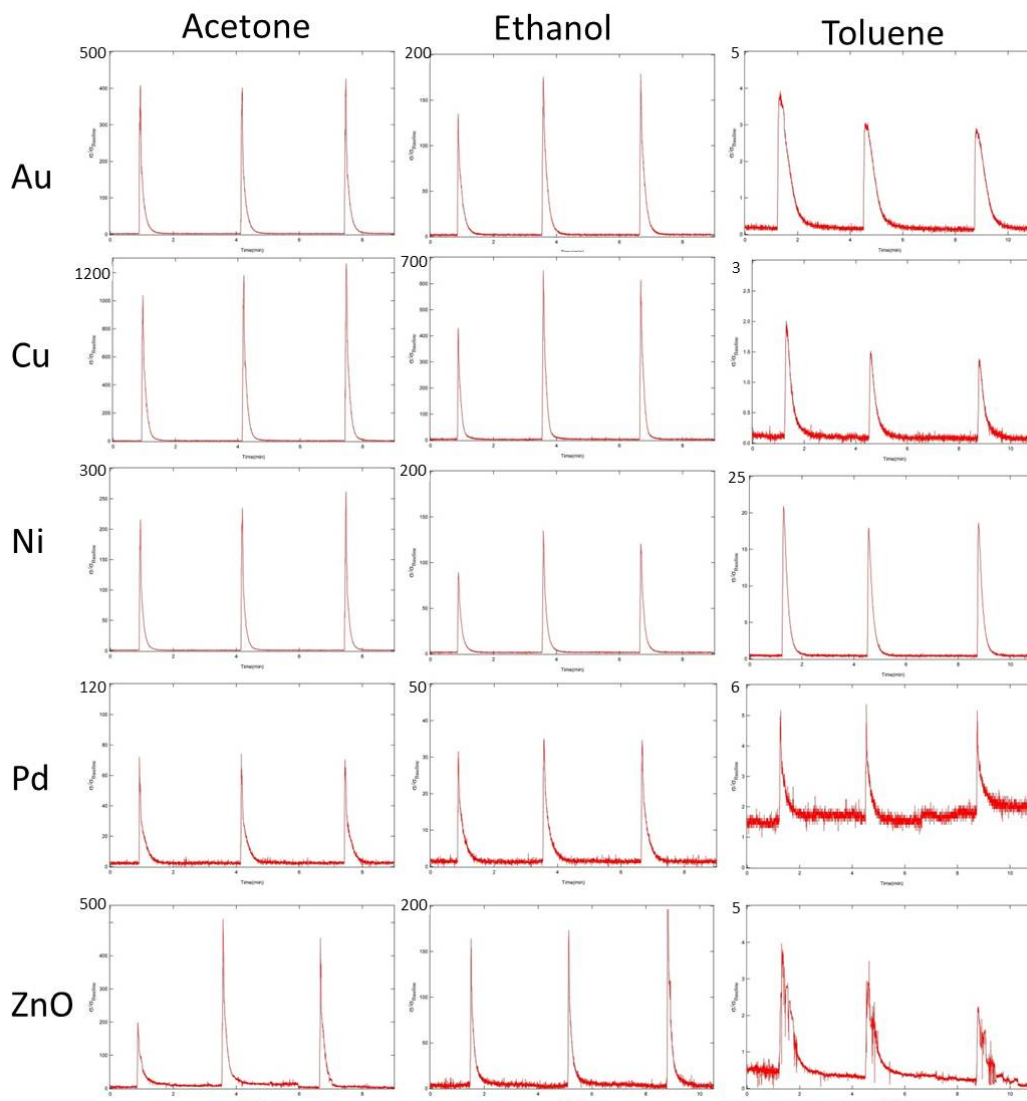
Figure 3.2 Exposure of the various nanospring elements to ~200 ppm Acetone, Ethanol and Toluene.

3.3 Limits of Detection

To effectively determine the detection limit of the various chemiresistors, the sublimation of solids is preferable to the evaporation of liquids. The VaporJet's ability to sublimate solids near instantaneously allows for extremely short pulses on the order of milliseconds [43]. The performance of the Pd/ZnO nanospring sensors with the optimal ZnO coating heated to 400 °C were tested using the VaporJet with the explosives

trinitrotoluene (TNT) and triacetone triperoxide (TATP). These compounds were introduced into the flow of artificial atmosphere in 0.1ms pulses. Repeatable peaks of conductance were obtained for both chemicals at the ppb levels of concentrations. A display of the responses at these levels is displayed in figure 9. These results provide evidence for the sensitivity of the sensor to extremely low levels of analyte concentrations under short exposure times (~0.1ms). With these exposure parameters, the sensors demonstrated a recovery time between 20 and 40s, significantly less than previously reported designs. [13-22].
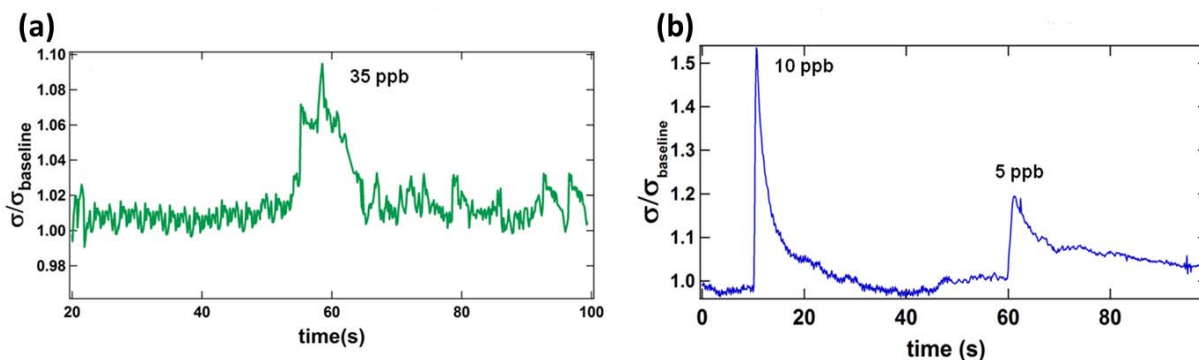
Figure 3.3 limits of detection using ZnO with Pd nanoparticles for (a) TATP and (b) TNT.

3.4 Selectivity

Selectivity between chemicals was achieved through the use of mutual information amongst sensors composed of different functional materials. Both LDA and PCA produced distinct regions for each gas; however, LDA proved to be superior in generating class separation. A comparison of LDA and PCA projections on a 5 sensor array is displayed in figure 3. PCA projections are used to demonstrate the ability of a

sensor to generate unique signals upon interaction with different analytes and is generally

not used to prepare data for classification.

Sum of mean distance: 4.29
Sum of variance: 0.207

Sum of mean distance: 7.13
Sum of variance: 0.063
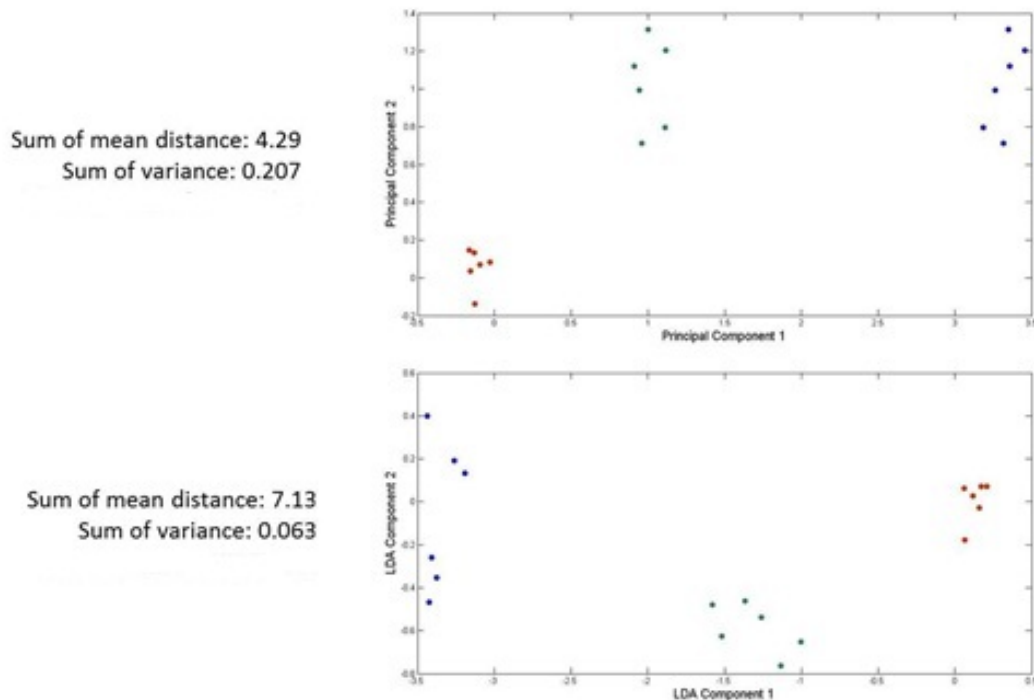
Figure 3.4 Comparison of PCA (top) and LDA(bottom) pre-processing techniques. LDA produces more distinct regions among the different classes.

Upon increasing the number of functional materials used (i.e. number of different

metallic nanoparticles) the discrimination power of the sensor array substantially

improved. For the present study, discrimination power is defined in the two dimensional

LDA space to allow direct comparison between any number of unique sensor elements.

Improved discrimination may be achieved by performing classification in higher

dimensional space, however, the two dimensional LDA space proved sufficient to

demonstrate the trends associated with increasing the number of functional materials used

in a sensor array. Furthermore, the use of two dimensional data for a classification

algorithm allows for facile computation and visualization. In the results that follow, discrimination power is defined in the two dimensional LDA space as follows:

$$D_p = \frac{\Sigma_{i,j} \mu_{ij}}{\Sigma_i \sigma_i}, \text{ where}$$

μ_{ij} represents distance between the means of class i and j, and σ_i the covariance of class i. The discrimination power for many sensors and features was calculated to determine which features provide maximum discrimination. Absorption rates were defined as area under the absorption curve divided by the time to max response; desorption rates were calculated in a similar manner using area under the desorption curve and time to baseline return. The magnitude of response of functionalized ZnO layers were normalized to the response of bare ZnO before calculating discrimination power. Finally, an exponential fit was performed on the absorption curves in an attempt to improve discrimination capability. For the exponential fit, the rate parameter provided the components of the corresponding input feature vector.

Experimental results imply that absorption rates for the sensor array provide maximum discrimination for the features tested. Improvements in the discrimination ability of the sensor array as the number of functional materials increased are visually discernible and displayed in figure 3.5.

(a) Sum of mean distance: 6.58
Sum of Variance : 0.119
Discrimination Power: 55.3

(b) Sum of mean distance: 6.29
Sum of Variance : 0.102
Discrimination Power: 61.6

(c) Sum of mean distance: 7.13
Sum of Variance : 0.063
Discrimination Power: 113.2
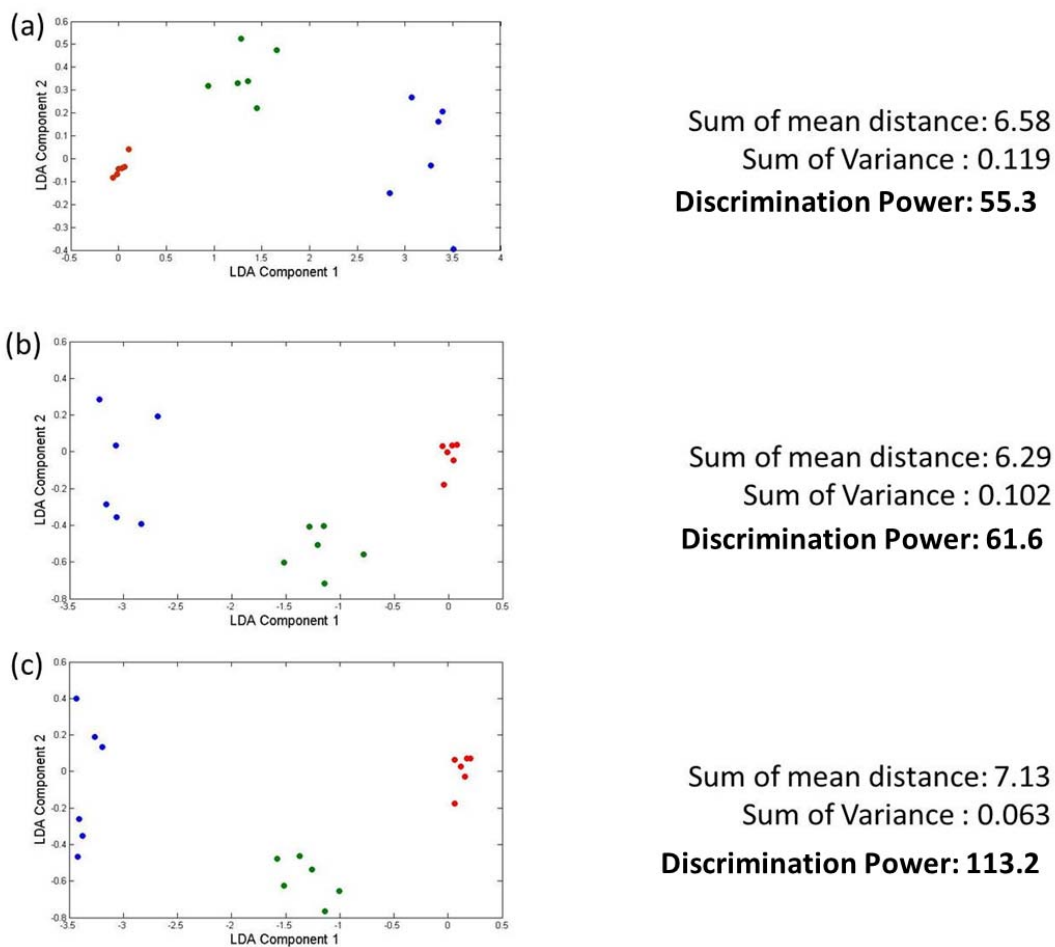
Figure 3.5 Two dimensional LDA plots for (a) an array of bare ZnO, Au, and Cu nanoparticles, (b) ZnO, Au, Cu, and Ni nanoparticles, (c) ZnO, Au, Cu, Ni and Pd nanoparticles. Increasing the number of functional materials divided the classes into more distinct regions.

A similar analysis was performed for desorption rates, magnitudes of response, and the exponential fit parameters with discrimination power results displayed in figure 3.5. It is important to note that regardless of the features used, increasing the number of functional materials used in the sensor array increased discrimination power. By extending the concept of discrimination power into more dimensions, discrimination

drastically improved, however, the computational cost to perform discrimination also increased with a magnitude dependent on the classification algorithm used.

	Sensor Components	Discrimination
Desorption Rates	ZnO, Au, Cu:	9.83
	ZnO, Au, Cu, Ni:	15.7
	ZnO, Au, Cu, Ni, Pd:	45.8
Normalized Magnitudes	ZnO, Au, Cu:	0.84
	ZnO, Au, Cu, Ni:	3.91
	ZnO, Au, Cu, Ni, Pd:	4.10
Exponential Rates	ZnO, Au, Cu:	3.25
	ZnO, Au, Cu, Ni:	9.68
	ZnO, Au, Cu, Ni, Pd:	31.7

Figure 3.6 Discrimination power calculated for different features of the conductometric signals in two dimensional LDA space.

The evaluation of features described above may be used as a reference in future research when performing classification based a subset of features.

3.5 Classification

3.5.1 Minimum Distance Classifier

Features extracted from the sensing elements were fed into a pattern recognition scheme to form decision regions capable of classifying a sensor response as one of the chemicals within the system's library. A straightforward method of forming a decision region is through a minimum distance classifier. In this classification scheme, features are

extracted from a response and assigned to the class with the minimum distance between

the class mean value and the projected feature. In this scenario, classes may be

discriminated visually by treating each sensor as an orthogonal axes and plotting

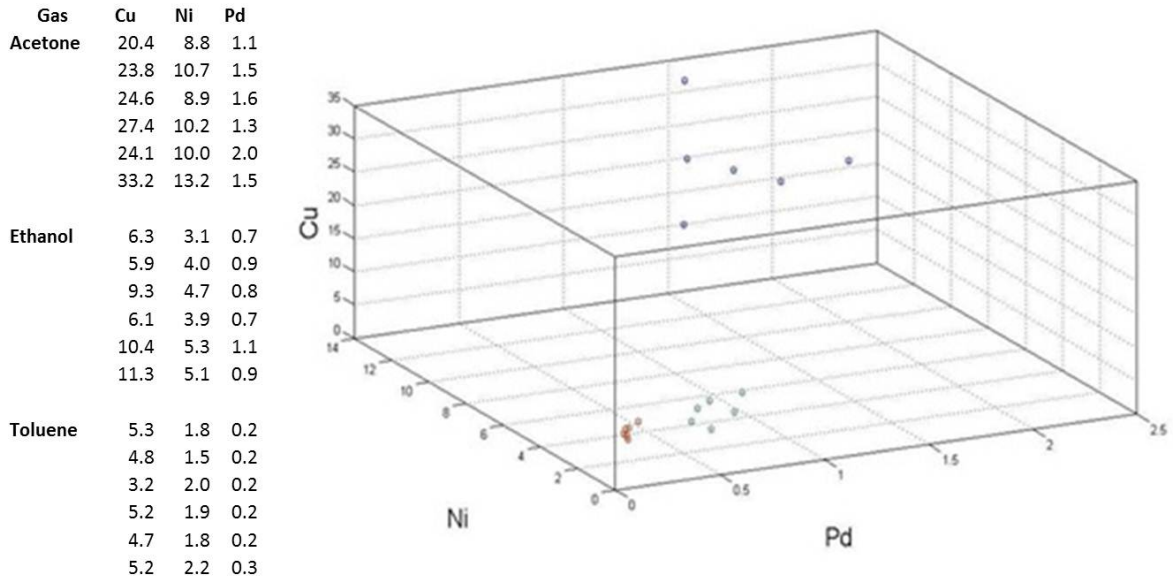responses against each other. A visual of such a plot is displayed in figure 3.7.

Gas	Cu	Ni	Pd
Acetone	20.4	8.8	1.1
	23.8	10.7	1.5
	24.6	8.9	1.6
	27.4	10.2	1.3
	24.1	10.0	2.0
	33.2	13.2	1.5
Ethanol	6.3	3.1	0.7
	5.9	4.0	0.9
	9.3	4.7	0.8
	6.1	3.9	0.7
	10.4	5.3	1.1
	11.3	5.1	0.9
Toluene	5.3	1.8	0.2
	4.8	1.5	0.2
	3.2	2.0	0.2
	5.2	1.9	0.2
	4.7	1.8	0.2
	5.2	2.2	0.3

Figure 3.7 Plot of absorption rates for three different nanoparticles plotted against one another. Clusters of points represent the response to the three gasses tested.

From the above figure, it is clear that each class occupies its own region;

however, decision boundaries for such a data set are complex and computationally

expensive to compute when the number of sensors is large. To combat this problem of

"the curse of dimensionality", LDA may be performed to maintain maximum separation

between classes while simultaneously reducing the dimensionality of the data. The

reduced dimensionality of the data allows for increased manageability and more efficient

computation times. Furthermore, any number of sensors may be used and their LDA

projections reduced to the desired dimensionality for computational efficiency.

A simple classifier based on minimum distance to the various class means in LDA space may be constructed using both distance metrics mentioned previously. Such a classifier applied to the absorption rates of nanosprings coated by bare ZnO, and bare ZnO functionalized with Au, Cu, Ni and Pd nanoparticles produced the following decision regions within the two dimensional LDA space:
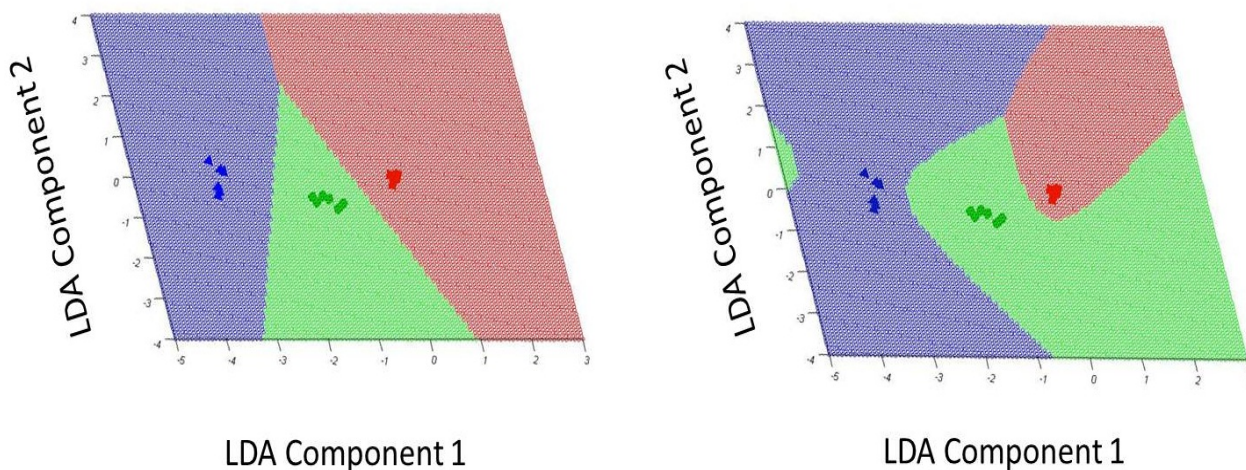

Figure 3.8 Minimum distance classifier boundaries for a five sensor array in two dimensional LDA space using Mahalnobis distance (right) and Euclidean (left). An exposure projected into the LDA space will be classified as toluene if it lies in the region occupied by the red squares, ethanol if in region occupied by the green circles, and acetone when in the region occupied blue triangles.

3.5.2 K-Nearest Neighbor

Implementing the minimum distance classifier into the kNN classification system yielded more local regions than other methods. The following classification region is generated for a scheme classifying an unknown sample by the class of its 3 nearest neighbors.
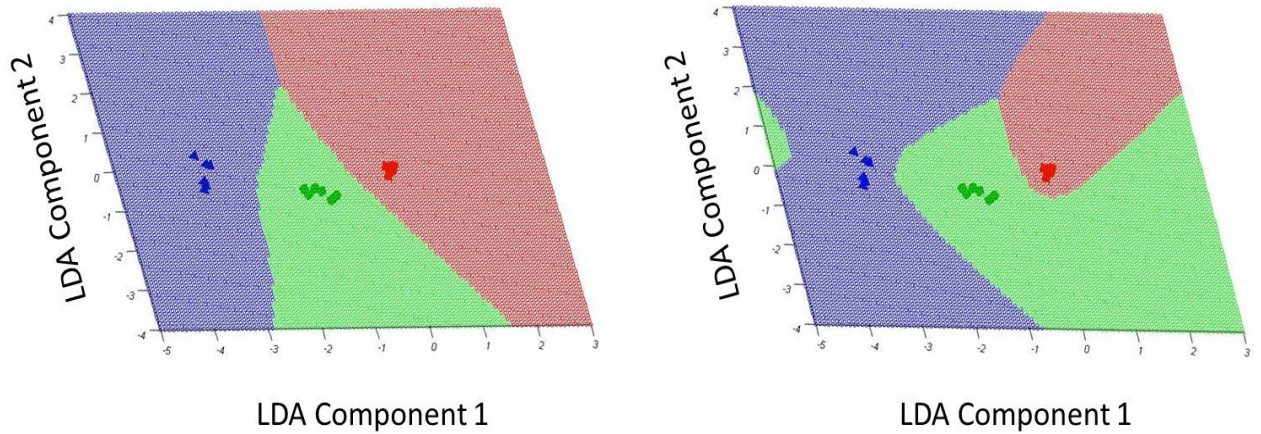
Figure 3.9 kNN classification regions for 3 nearest neighbors using the Mahalanobis distance metric (right) and Euclidian metric (left).

3.5.3 Multivariate Gaussian

Using the LDA data as a basis, a normal distribution for each class may be constructed and used to form distinct regions for each class. Modeling the two dimensional LDA data of figure 3.4(c) with the standard multivariate normal distribution yields the probability distributions described in figure 3.5. The z-value indicates the probability that a projected point lying at the corresponding (x,y) coordinate belongs to each class, indicated by color.
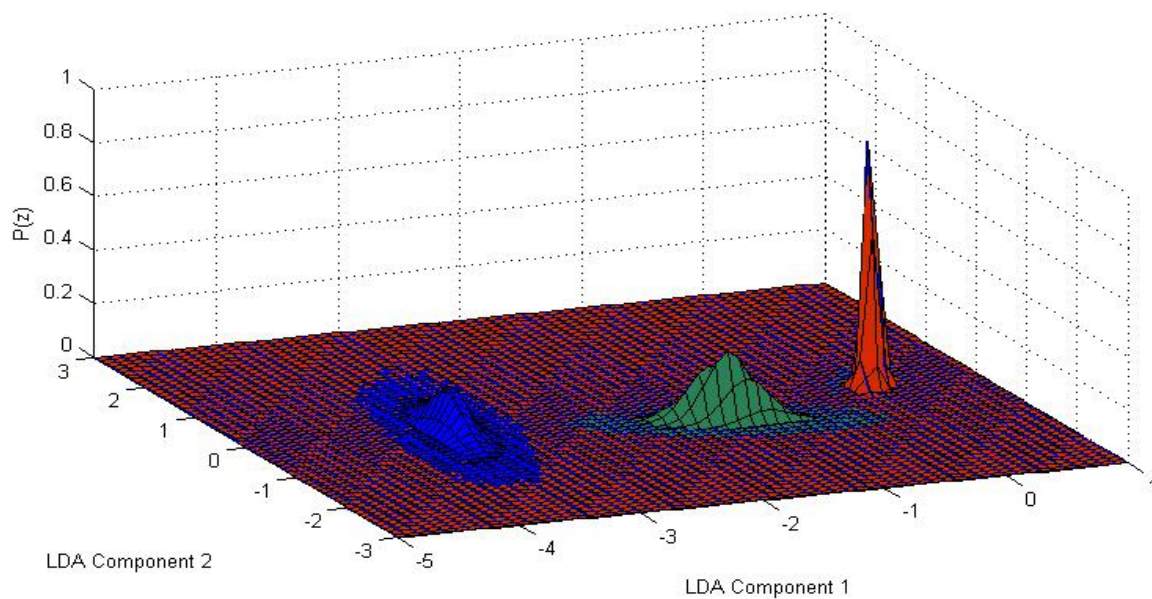
Figure 3.10 Plot of the normal probability distributions for each LDA class.

Using the associated probability distributions, decision regions may be formed at the boundaries where the probability of a projected point belonging to more than one class is equal (e.g. P(ethanol) = P(toluene)). This results in distinct regions for the two classes with the least variance (or "spread") and a default region belonging to the class with highest variance. This default region may be removed through the application of a threshold value below which the algorithm classifies the sample as "unknown". A depiction of decision regions generated through Gaussian analysis is demonstrated in figure 3.11.
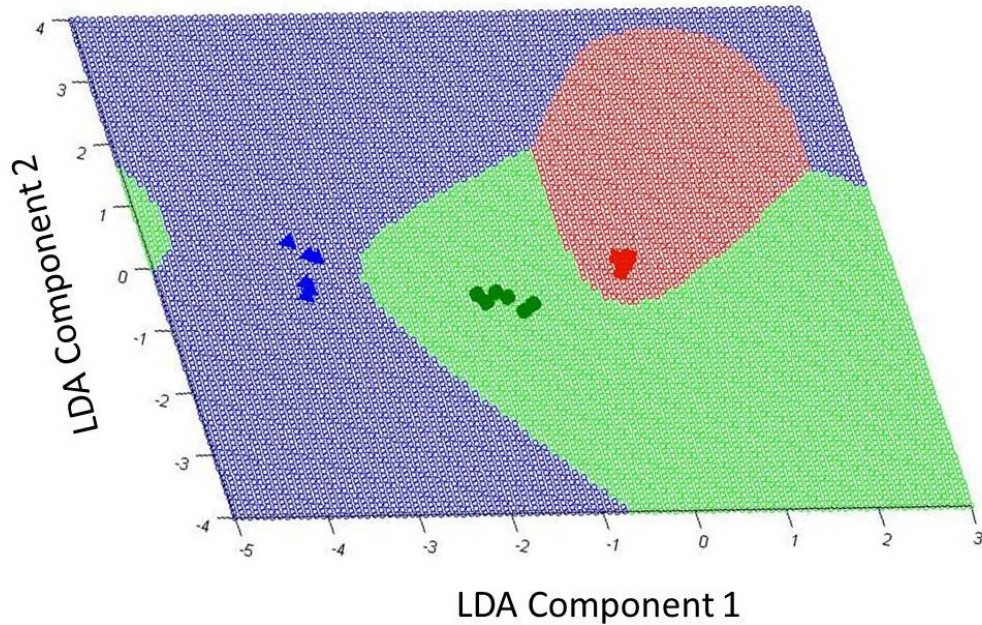
Figure 3.11 Decision regions formed using the Multivariate Guassian technique applied to the five sensor array in fig 3.4(c).

Using these regions, an unknown sample may be characterized by first projecting its features using the projection vector obtained through linear discriminant analysis and then performing classification based on the class with the highest probability for the selected points.

3.6 Room Temperature Sensitivity

After determining that the sensing element under study is capable of explosive detection and discrimination, efforts were made to improve the sensor's performance by utilizing the optical properties of ZnO. At room temperature, exposure of ZnO coated nanosprings to UV light with a peak intensity of 385nm increased the conductance of the mat by a factor of eight, as shown in figure 3.7. This increased conductance is due to the

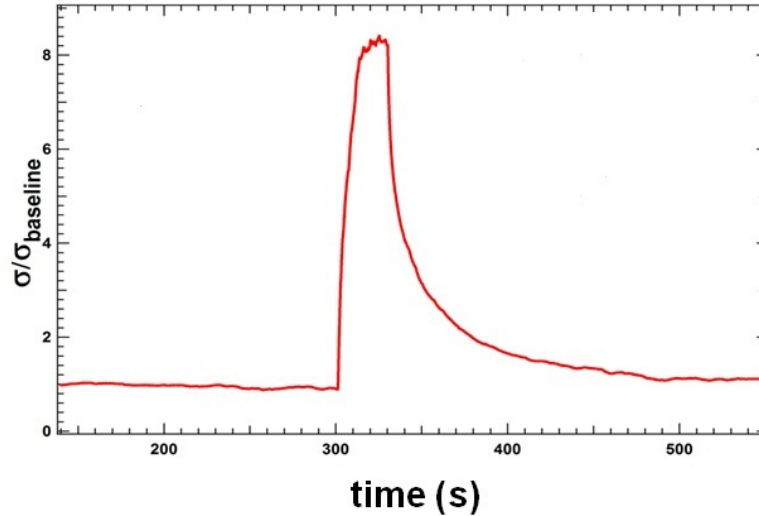enhanced carrier density and decreased depletion width within the ZnO layer upon exposure to UV light.

Figure 3.12 ZnO coated nanosprings exposed to UV light (peak intensity 385nm) at a temperature of 25 $^{\circ}$C. Upon exposure an increase in conductance by a factor of 8 was observed.

Using the mechanisms discussed in section 1.3, the sensing properties of UV activated nanospring sensors were studied. In this study, the nanospring sensor was exposed to UV light until a steady-state baseline was achieved. Exposures to ~500ppm Toluene, Ethanol, and Acetone were performed and are displayed in figure 3.8. It was found that the UV-activated sensor responds to a vapor pulse with significantly less noise and returns to baseline faster than thermally-activated sensors. However, the level of response is more than 10 times lower than the response of its thermally activated counterpart.
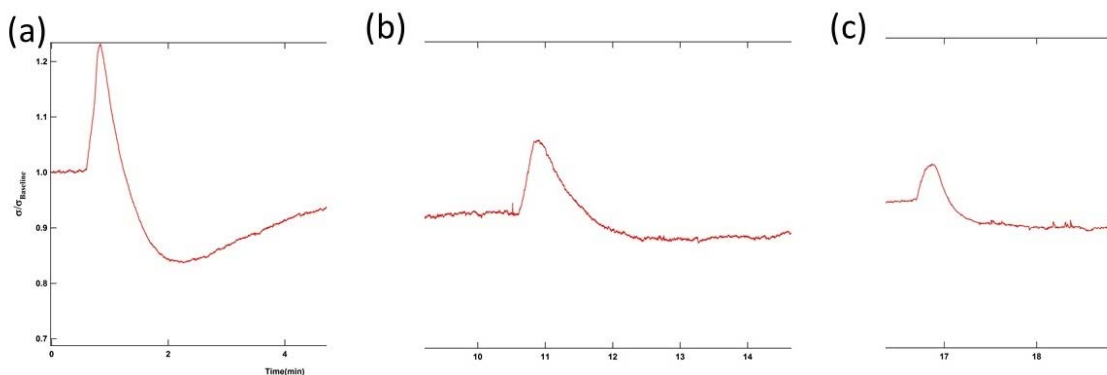
Figure 3.13 UV activated ZnO nanosprings coated with Au NPs exposed to (a) Acetone, (b) Ethanol, and (c) Toluene.

3.7 UV activation to Increase Refresh Rate

Sensitivity and selectivity, while being the most important factors of a sensing element, are not the only parameters to consider when constructing a gas sensor. The level of noise and baseline stability is also substantially important parameters that affect overall sensor performance. Baseline stability refers to the ability of a sensor to oxidize analyte vapors and restore oxygen coverage. Due to the fast evaporation of most catalytic reaction products from the nanospring surface, nanospring-based sensors are in general self-refreshing and do not require a reset mechanism. However, for exposures to complex organic analytes, such as TNT, the time for baseline restoration may be long – significantly impeding the ability of the sensor to perform multiple measurements in a short amount of time.

To combat this long refresh time, UV exposure was investigated as a means of reducing the refresh time upon exposure to TNT. This choice of chemical was made because TNT ($C_7H_5N_3O_6$) is capable of full catalytic oxidation into products of carbon

dioxide, water, and nitrogen gas. However, TNT has a significant number of intermediate

oxidation products which substantially increase the time of reaction by remaining

attached to surface defects and oxidizing at a slower rate to the final oxidation products.

These intermediate reaction products may be dissociated by UV light, leading to a

quicker oxidation and hence faster baseline restoration. Similarly, high energy electrons

generated by UV light are capable of ionizing atmospheric oxygen, increasing the rate at

which oxygen vacancies left by the redox reactions with TNT and its reaction products

repopulate. These two processes contribute to a decrease in recovery time and the results

of UV activation after exposure to a pulse of TNT are shown in figure 3.9.
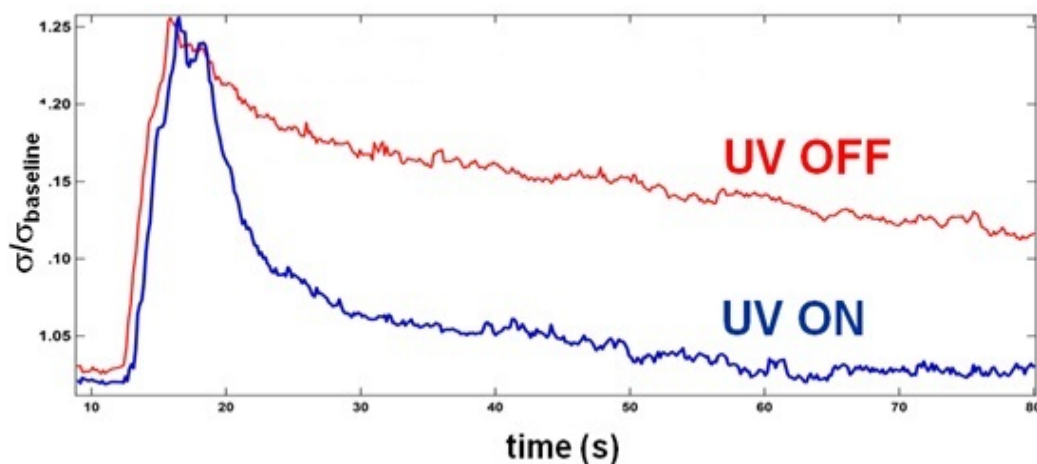
Figure 3.14 Response of thermally activated ZnO coated nanosprings decorated
with Pd nanoparticles exposed to TNT (red) and TNT followed by irradiation of
UV light (blue). The sensor was heated to a temperature of 400 $^{\circ}$C and exposed to
a concentration of 5 ppb TNT.

3.8 Conclusions and Future Work

Nanospring structures provide a suitable substrate for depositing gas sensitive

materials as sensor elements in an electronic nose system. An array of nanospring mats

functionalized with a thin film of ZnO and a variety of metallic nanoparticles offer extremely sensitive sensor elements for detecting explosive vapors in concentrations as low as 5 ppb. By using an array of these sensor elements, discrimination between various explosive chemical species may be achieved. It has been shown that any common pattern recognition technique may be used in conjunction with the nanospring sensor array to provide classification. The above decision regions have been implemented into data acquisition software for real time analysis of chemicals in the environment. Discrimination between the three chemicals tested was achieved with 100% efficiency for high concentrations of the analyte (100s of ppm); however, the ability to distinguish between low concentrations of these chemical species (<10 ppm) or mixtures of them remains a challenge.

Future research in this field should focus on solutions to this challenge. Such research must adopt a multidisciplinary approach to investigate optimal functional materials and processing techniques for the nanospring sensor elements. This research must also include investigations into the use of advanced pattern recognition techniques, such as neural networks or support vector machines. Discrimination power rankings of the various features with LDA may provide a starting point for the design of these future pattern recognition systems

Upon completion of the above tasks, work into the design of a portable electronic nose system utilizing these nanospring sensing elements provides the potential for detecting explosive materials in the field. As this thesis has already demonstrated, small, cost-effective conductometric sensors composed of nanospring elements are capable of identifying trace quantities of IED materials and their degradation products. Further

research into expanding both the sensitivity and selectivity of the sensing elements may lead to the design of an effective, portable bomb detector capable of replacing the canine in "sniffing" out explosive threats.

REFERENCES

[1] T.C. Pearce, S.S. Schiffman, H.T. Nagle, J.W. Gardner, *Handbook of Machine Olfaction - Electronic Nose Technology,* John Wiley & Sons, 2003

[2] K. Arshak, E. Moore, G.M. Lyons, J. Harris, S. Clifford, *A review of gas sensors employed in electronic nose applications*, Sensor Review **24,** 181-198 (2004)

[3] J. Yinon, *Detection of explosives by electronic noses*, Anal. Chem. **75**, 98A-105A (2003)

[4] V. Dobrokhotov, L. Oakes, D. Sowell, A. Larin, J. Hall, A. Kengne, P. Bakharev, G. Corti, T. Cantrell, T. Prakash, J. Williams, and D.N. McIlroy, *ZnO coated nanospring-based chemiresistors*, Journal of Applied Physics, **111** (2012)

[5] V. Dobrokhotov, L. Oakes, D. Sowell, A. Larin, J. Hall, A. Kengne, P. Bakharev, G. Corti, T. Cantrell, T. Prakash, J. Williams, and D.N. McIlroy, *Toward the nanospring-based artificial olfactory system for trace-detection of flammable and explosive vapors*, Sensors and Actuators B: Chem http://dxi.doi.org/10.1016/j.snb.2012.03.074 (2012)

[6] V.V. Dobrokhotov, D.N. McIlroy, G. M. Norton, R. Abdelrahaman, A. Safir, and C.A. Berven, *Interaction of Hybrid Nanowire–Nanoparticle Structures with Carbon Monoxide*, Nanotechnology **20** 135504 (2009)

[7] C. A. Berven, and V. V. Dobrokhotov, *Towards practicable sensors using one dimensional nanostructures,* International Journal of Nanotechnology **5** 402-449 (2007)

[8] V.V. Dobrokhotov, D.N. McIlroy, M. G. Norton, and C.A. Berven, *Transport properties of hybrid nanoparticle-nanowire systems and their application to gas sensing,* Nanotechnology **17** 4135–4142 (2006)

[9] V.V. Dobrokhotov, D.N. McIlroy, M. G. Norton, A. Abuzir, W. J. Yeh, I. Stevenson, R. Pouy, J. Bochenek, M. Cartwright, L. Wang, J. Dawson, M. Beaux, and C. A. Berven, *Principles and Mechanisms of Gas Sensing by GaNNanowires Functionalized with Gold Nanoparticles,* Journal of Applied Physics **99** 104302 (2006)

[10] D. N. McIlroy, A. Alkhateeb, D. Zhang, D. E. Aston, A. C. Marcy, and M. G. Norton, *Nanospring Formation - Unexpected Catalyst Mediated Growth,* Journal of Physics: Condensed Matter **16** R415-R440 (2004)

[11] L. Wang, D. Major, P. Paga, D. Zhang, M. G. Norton, and D. N. McIlroy, *High Yield Synthesis and Lithography of Silica-Based Nanospring Mats*, Nanotechnology **17** S298-S303 (2006)

[12] D. Zhang, A. Alkhateeb, H. Han, H. Mahmood, and D.N. McIlroy, *Silicon Carbide Nanosprings*, Nano Letters **5** 983-987 (2003)

[13] Y.S. Choe, *New gas sensing mechanism for SnO$_2$ thin-film gas sensors fabricated by dual ion beam sputtering,* Sensors and Actuators B **8** 200-208 (2001)

[14] V. Sysoev, J.Goschnick, T. Schneider, E. Strelcov, and A.Kolmakov *A Gradient Microarray Electronic Nose Based on Percolating SnO2 Nanowire Sensing Elements,* Nano Letters **7** 3182 - 3188 (2007)

[15] C. Wang, L. Yin, L. Zhang, D. Xiang, R. Gao, *Metal Oxide Gas Sensors: Sensitivity and Influencing Factors*, Sensors **18** 2088 (2010)

[16] H.W. Ra, R. Khan, J. T. Kim, B.R. Kang and Y.H. Im, *The effect of grain boundaries inside the individual ZnO nanowires in gas sensing,* Nanotechnology **21** 085502 (2010)

[17] S. Roy and S. Basu, *Improved zinc oxide film for gas sensor applications*, Bull. Mater. Sci. **25** 513 – 515 (2002)

[18] A. P. Chatterjee, P. Mitra, A. K. Mukhopadhyay, *Chemically deposited zinc oxide thin film gas sensor,* Journal of Materials Science **34** 4225 – 4231(1999)

[19] A. Cabot, A. Vilà, J.R. Morante, *Analysis of the catalytic activity and electrical characteristics of different modified SnO$_2$ layers for gas sensors*, Sensors and Actuators B **84** 12-20 (2002)

[20] V. V. Sysoev, I. Kiselev, M. Frietsch, and J. Goschnick, *Temperature Gradient Effect on Gas Discrimination Power of a Metal-Oxide Thin- Film Sensor Microarray,* Sensors **4** 37-46 (2004)

[21] L. Liao, H.B. Lu, J.C. Li, H. He, D.F. Wang, D.J. Fu, C. Liu, *Size dependence of gas sensitivity of ZnO nanorods,* Journal of Physical Chemistry C **111** 1900-1903 (2007)

[22] N. Barsan and U. Weimar, *Conduction Model of Metal Oxide Gas Sensors,* Journal of Electroceramics, **7** 143–167 (2001)

[23] N. Barsan and U Weimar, *Understanding the fundamental principles of metal oxide based gas sensors; the example of CO sensing with SnO2 sensors in the presence of humidity*, J. Phys.: Condens. Matter **15** R813–R839 (2003)

[24] V.P. Zhdanov, *nm-sized Particles on a Semiconductor Surface, Schottky Model, etc.*, Surface Sciences **3** L331-L334

[25] S.V. Ryabstev, E.A. Tutov, E.N. Bormontov, A.V. Shaposhnik, and A.V. Ivanov, *Interaction of Metal Nanoparticles with a Semiconductor in Surface-Doped Gas Sensors*, Semiconductors **4** 869-873 (2001)

[26] A. Kolmakov, D. O. Klenov, Y. Lilach, S. Stemmer, and M. Moskovits, *Enhanced Gas Sensing by Individual SnO2 Nanowires and Nanobelts Functionalized with Pd Catalyst Particles,* Nano Lett. **5** 667-673 (2005)

[27] C. Quinn and M. Roberts, *Chemisorption of oxygen and subsequent process on metal films: work function measurements*, Trans. Faraday Soc. **60** 899-912 (1964)

[28] S.Fan, A. K. Srivastava, and V. P. Dravid*, UV-Activated Room-Temperature Gas Sensing Mechanism of Polycrystalline ZnO*, Applied Physics Letters **95** 142106 (2009)

[29] Q. H. Li, T. Gao, Y. G. Wang, and T. H. Wang, *Adsorption and Desorption of Oxygen Probed from ZnO Nanowire Films by Photocurrent Measurements*, Applied Physics Letters **86** 123117 (2005)

[30] Lei Luo, Brian D. Sosnowchik and Liwei Lin, *Local Vapor Transport Synthesis of Zinc Oxide Nanowires for Ultraviolet-Enhanced Gas Sensing*, Nanotechnology **21** 495502 (2010)

[31] J. Y. Park, D. E. Song and S.S. Kim, *An Approach to Fabricating Chemical Sensors Based on ZnO Nanorod Arrays*, Nanotechnology **19** 105503 (2008)

[32] R. G. Osuna, *Pattern Analysis for Machine Olfaction: A Review,* IEEE Sensors **13** 189-202 (2002)

[33] L. Carmel, S. Levy, D. Lancet, D. Harel, *A feature extraction method for chemical sensors in electronic nose*, Sensors and Actuators B **93** 67-76 (2003)

[34] L. Carmel, N. Sever, D. Lancet, and D. Harel, *An eNose Algorithm for Identifying Chemicals and Determining their Concentration*, Sensors and Actuators B **17** (2002)

[35] H. Hong, C.H. Kwon, S. Kim, D. H. Yun, K. Lee, Y . K. Sung, *Portable electronic nose system with gas sensor array and artificial neural network*, Sensors and Actuators B **66** 49-52 (2000)

[36] L. Carmel, N. Sever, D. Lancet, D. Harel, *An eNose algorithm for identifying chemicals and determining their concentration*, Sensors and Actuators B **93** 77-83 (2003)

[37] M. E. Koscho, R. H. Grubbs, N. S. Lewis, *Properties of Vapor Detector Arrays Formed through Plasticization of Carbon Black−Organic Polymer Composites,* Anal. Chem. **7** 1307–1315 (2002)

[38] O. K. Varghese, P. D. Kichambre, D. Gong, K. G. Ong, E. C. Dickey and C. A. Grimes, *Gas Sensing Characteristics Of Multi-Wall Carbon Nanotubes,* Sensors and Actuators B **81** 32-41 (2001)

[39] H. Schaefer, *Nanoscience: The Science of the Small in Physics, Engineering, Chemistry, Biology, and Medicine,* Springer (2010)

[40] J. Mainland and N. Sobel, *The Sniff is Part of the Olfactory Percept*, Chemical Senses **31** 181-196 (2006)

[41] I. Gazit, J. Terkel, *Domination of Olfaction Over Vision in Explosives Detection by Dogs*, Applied Animal Behaviour Science **9** 65-73 (2003)

[42] J. W. Elam and S. M. George, Growth of ZnO/Al2O3 Alloy Films Using Atomic Layer Deposition Techniques, *Chemistry of Materials* **15** 1020-1028 (2003)

[43] B. Antohe, D. J. Hayes, S. Ayers, D.B. Wallace, M. E. Grove, and M. Christison, *Portable Vapor Generator for the Calibration and Test of Explosive Detectors,* 2009 IEEE International Conference on Technologies for Homeland Security

[44] V. Dobrokhotov, L. Oakes, D. Sowell, A. Larin, J. Hall, A. Kengne, P. Bakharev, G. Corti, T. Cantrell, T. Prakash, J. Williams, and D.N. McIlroy *Thermal and Optical Activation of the Nanospring-Based Chemiresistors,* Sensors 14792 Accepted for publication.